Nanoscale

ROYAL SOCIETY OF CHEMISTRY

REVIEW

View Article Online
View Journal | View Issue

Cite this: *Nanoscale*, 2024, **16**, 14033

Theranostic nanogels: multifunctional agents for simultaneous therapeutic delivery and diagnostic imaging

Ismail Altinbasak, [a] Yasin Alp,[a] Rana Sanyal[a,b] and Amitav Sanyal *[a,b]

In recent years, there has been a growing interest in multifunctional theranostic agents capable of delivering therapeutic payloads while facilitating simultaneous diagnostic imaging of diseased sites. This approach offers a comprehensive strategy particularly valuable in dynamically evolving diseases like cancer, where combining therapy and diagnostics provides crucial insights for treatment planning. Nanoscale platforms, specifically nanogels, have emerged as promising candidates due to their stability, tunability, and multifunctionality as carriers. As a well-studied subgroup of soft polymeric nanoparticles, nanogels exhibit inherent advantages due to their size and chemical compositions, allowing for passive and active targeting of diseased tissues. Moreover, nanogels loaded with therapeutic and diagnostic agents can be designed to respond to specific stimuli at the disease site, enhancing their efficacy and specificity. This capability enables fine-tuning of theranostic platforms, garnering significant clinical interest as they can be tailored for personalized treatments. The ability to monitor tumor progression in response to treatment facilitates the adaptation of therapies according to individual patient responses, highlighting the importance of designing theranostic platforms to guide clinicians in making informed treatment decisions. Consequently, the integration of therapy and diagnostics using theranostic platforms continues to advance, offering intelligent solutions to address the challenges of complex diseases such as cancer. In this context, nanogels capable of delivering therapeutic payloads and simultaneously armed with diagnostic modalities have emerged as an attractive theranostic platform. This review focuses on advances made toward the fabrication and utilization of theranostic nanogels by highlighting examples from recent literature where their performances through a combination of therapeutic agents and imaging methods have been evaluated.

Received 1st April 2024,
Accepted 2nd July 2024

DOI: 10.1039/d4nr01423e

rsc.li/nanoscale

1. Introduction

Theranostic agents constitute an emerging class of materials that integrate diagnosis and therapy within a single platform.[1–4] In recent years, the theranostic approach has garnered increasing interest, as it aims to achieve targeted delivery of patient-specific medication. Incorporating a diagnostic component into the therapeutic agent delivery system offers insights into the localization of the drug carrier at the disease site and the disease's state during therapy. Despite diseases being categorized into specific types and patient sub-populations, their nature can vary significantly among individuals due to disease heterogeneity. In complex diseases like cancer, where each case may exhibit unique characteristics, theranostics can enhance therapy by tailoring it to the individual patient. Consequently, the integration of diagnostics and therapy holds promise in providing clinicians with a comprehensive understanding of disease progression in each patient, enabling them to offer more informed and personalized treatment.

Over the past decades, it has been well established that nanosized delivery platforms can effectively combine diagnostic and therapeutic agents into a single platform, capable of passively or actively targeting the disease site. Despite seeming trivial, the size of nanoparticles plays a critical role in both drug delivery and imaging. Nanosized particles selectively accumulate in tumor tissue rather than healthy tissue due to the disorganized nature of cancer cells, leading to the enhanced permeability and retention effect (EPR).[5] These nanosized delivery agents are recognized for providing solutions to classic problems such as the low solubility of most conventional drugs and slowing down their rapid systematic clearance.[6–8] In this manner, drug formulations containing

[a]*Department of Chemistry, Bogazici University, Bebek, Istanbul 34342, Türkiye. E-mail: amitav.sanyal@bogazici.edu.tr*
[b]*Center for Life Sciences and Technologies, Bogazici University, Bebek, Istanbul 34342, Türkiye*

nanoparticles can enhance drug bioavailability, stability, and pharmacokinetic profile. In recent years, various nanoparticle constructs have been utilized in theranostic applications, including gold nanoparticles,[9] superparamagnetic iron oxide (SPION),[10] and quantum dots.[11] Conversely, nanosized polymeric particles such as micelles and liposomes have also emerged as versatile platforms offering various customizations such as multifunctionality, size and elasticity modulation, and stimuli responsiveness.[12,13] Additionally, the chemical composition of polymeric nanoparticles can be tailored to enable them to evade detection by the immune system and remain in stealth mode during *in vivo* delivery.[14]

While numerous polymeric nanoparticles have been investigated to date, interest in utilizing nanogels has been steadily increasing.[15–21] Compared to other nano-constructs, polymeric nanogels stand out as attractive candidates for theranostic platforms due to their unique properties. These include a rich diversity in the choice of polymer,[22] tunable nanoparticle size,[23] high drug loading capacity,[24] surface functionality,[25] and the ability to impart stimuli-responsive characteristics.[26–28] This versatility in design enables the engineering of systems with the desired combination of therapy and diagnostic modes. Common therapeutic approaches include chemotherapy agents, photodynamic/photothermal agents, and gene therapy, which can be combined with diagnostic modalities such as magnetic resonance imaging (MRI), optical imaging, photoacoustic imaging (PA), positron emission tomography (PET), and single-photon emission computed tomography (SPECT) (Scheme 1).

The ability to customize the amphiphilicity and chemical composition of polymers in soft nanoparticles like nanogels provides control over drug loading and release characteristics, as well as interactions with the biological environment, such as tuning biocompatibility and immune responses. Flexible polymer chains and a porous inner structure create a sponge-like material allowing high quantities of therapeutic and imaging agents to be loaded.[29,30] Crosslinked architectures prevent dissolution while maintaining nanogel integrity upon swelling or excessive dilution during administration. Although physical loading of drugs and imaging agents is often preferred, they can also be chemically conjugated to nanogels. A significant drawback of traditional chemotherapy, namely lack of specificity and toxicity to normal tissue, can be mitigated by conjugating targeting groups onto nanogel surfaces to enhance accumulation in cancerous cells. Additionally, nanogel constructs offer the advantage of adaptability, with

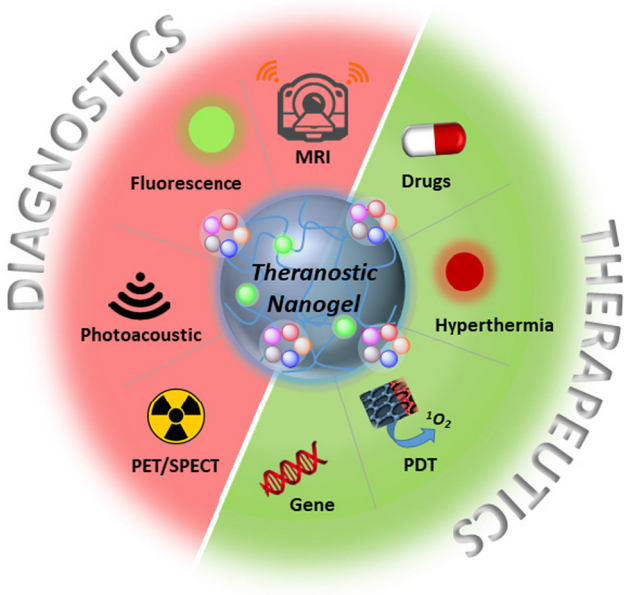

Scheme 1 Illustration of diagnostic and therapeutic modalities for theranostic nanogels.

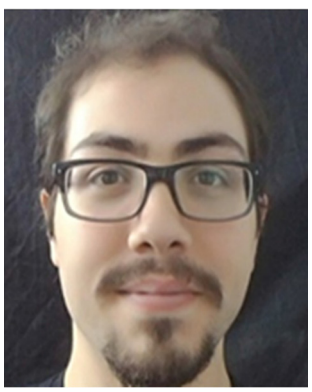

Ismail Altinbasak

Ismail Altinbasak received his undergraduate degree from the Department of Chemistry at Bogazici University, Istanbul, Türkiye. Thereafter, he obtained his M.S. degree in chemistry in 2016 under the supervision of Prof. Amitav Sanyal, working in the area of responsive hydrogels for protein delivery. Recently, Ismail obtained his doctoral degree in the Sanyal group, and now is pursuing his postdoctoral studies in Mayo Clinic, Phoenix, Arizona, USA. His interests include the design and fabrication of novel polymeric biomaterials ranging from nanofibers to nanogels for various biomedical applications such as combating bacterial infection to targeted drug delivery to cancer cells.

Yasin Alp

Yasin Alp received his B.Sc. degree in Chemistry (2021) from Bogazici University, where he worked in design and synthesis of pH-responsive electrospun nanofibers and redox-responsive polymeric materials in the Sanyal group. He is currently pursuing a Ph.D. at the University of Massachusetts Amherst. His research focuses on polymeric delivery systems for biologics and targeted protein degradation.

their physical and chemical behavior effectively altered in response to changes in the environment, triggered by exogenous or endogenous stimuli. Stimuli-responsive chemistries have opened new avenues in the design, synthesis, and applications of theranostic nanogels.[31] The drug release profile and imaging ability of nanogel systems can be enhanced by local conditions, biological triggers, and external stimuli such as changes in pH, temperature, redox potential, and light. These triggers facilitate focused and cumulative drug release, as well as improved imaging quality through contrast modulation.

Another crucial attribute of nanogels is their soft, sponge-like nature, which allows them to undergo size and shape changes in response to external forces.[32] Unlike hard nanoparticles, such as silica, gold, magnetic, and poly(L-lactic acid) nanoparticles, which maintain their size and shape during circulation, soft nanoparticles like nanogels can be compressed to traverse dense biological barriers and reach desired sites (Scheme 2).[33,34] Furthermore, studies have demonstrated that a higher proportion of soft particles remain in circulation due to their resistance to phagocytosis compared to their counterparts, enabling more particles to reach targeted tissues.[35,36] Consequently, these structural adaptations facilitate the development of an ideal theranostic system, characterized by selective release, advanced imaging capabilities, efficient targeting, and a favorable clearance rate.

Although significant effort has been invested in nanogels, numerous challenges persist in converting academic studies into commercial products. Many of the challenges encountered in the synthesis, characterization, and application of nanoparticles are also relevant for nanogels. Large-scale fabrication of nanogels presents different problems compared to small-scale laboratory synthesis. Additionally, achieving thorough and precise chemical characterization of nanoparticles can be difficult due to their complex structures, making it challenging to meet certain specification qualities of nanogels in both large- and small-scale production. Moreover, nanogels face similar challenges to nanoparticles when delivered into the bloodstream, including unguided distribution due to a lack of targeting ability unless specifically armed with a target-specific ligand, and uncontrolled biological processes such as corona formation, which are the main obstacles at the application site.[37]

This review article endeavors to offer a comprehensive overview of recent advancements in theranostic nanogels utilized for cancer diagnosis and therapy. It delves into the diverse array of natural and synthetic polymers employed in the fabrication of nanogels, while also exploring the synthetic methodologies utilized for crosslinking. In particular, the chemical compositions of the polymers employed to fabricate these nanogels have been highlighted for the examples discussed in detail. To provide the readers with an organized format, the article has been structured along the imaging modalities that are commonly employed. The articles highlighted herein are chosen using established search engines and are from recent literature. Although some examples where the function of such theranostic nanogels have been demonstrated only *in vitro* have been chosen, emphasis is given to studies that also have evaluation in an *in vivo* setting, a vital criterion for future translation to the clinic. Specifically, this review sheds light on nanogels that seamlessly integrate imaging and therapeutic modalities, presenting a promising avenue for enhanced

Rana Sanyal

Rana Sanyal graduated from Bogazici University with a B.S. degree in Chemical Engineering and continued her studies at Boston University receiving her Ph.D. degree in Chemistry. Prof. Sanyal started her career as a research scientist in Amgen Inc., California. Since 2004, she has been a faculty member at the Department of Chemistry at Bogazici University. Her current research interests focus on targeted drug delivery. Prof. Sanyal has been named one of the three Cartier Women's Initiative 2021 Global Science and Technology Pioneer Award fellows and the European Women Innovator in 2022. She is an inventor or co-inventor of over 50 issued patents or pending applications. Since 2013, she has been the director of the Center for Life Sciences and Technologies at Bogazici University. Rana Sanyal is also the Co-Founder and Chief Science Officer of RS Research, a clinical-stage biotechnology start-up developing novel nanomedicines.

Amitav Sanyal

Amitav Sanyal obtained his undergraduate degree from the Indian Institute of Technology in Kanpur, India. He received his Ph.D. from Boston University (USA), in the area of asymmetric organic synthesis. During post-doctoral work with Prof. Vincent M. Rotello at the University of Massachusetts at Amherst, USA, he worked in the area of renewable polymeric coatings. Currently, he is a professor in the Department of Chemistry at Bogazici University, Istanbul, Turkey. His research focuses on the design of novel polymeric materials such as coatings, hydrogels, and nanofibers for biomedical applications. His awards include the Young Investigator Award from the Turkish Academy of Sciences and TUBITAK (The Scientific and Technological Research Council of Türkiye).

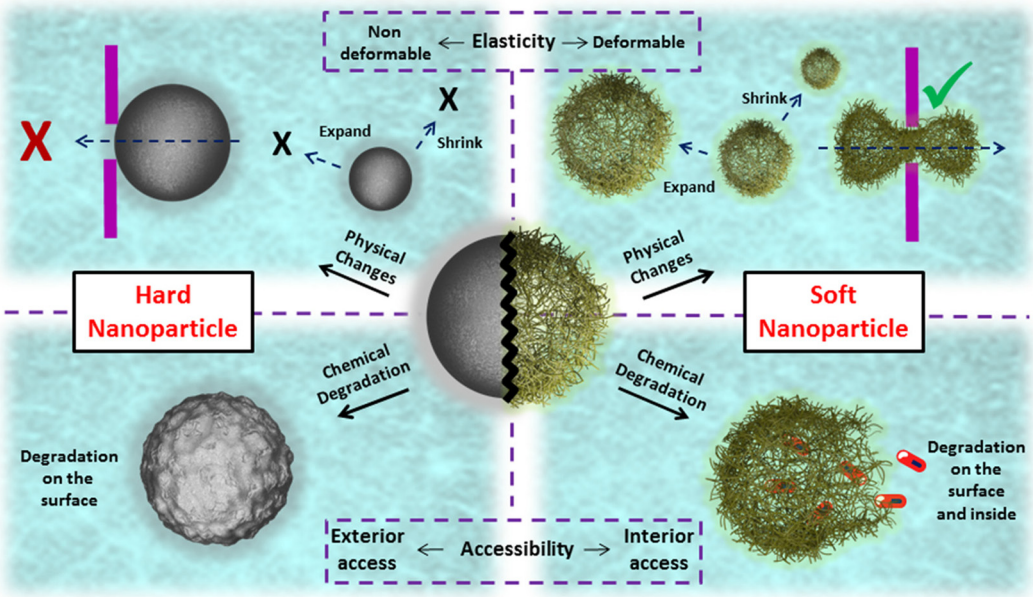

Scheme 2 Illustration of the behavior of hard and soft nanoparticles.

cancer management. Specifically, it examines the significance of stimuli-responsive properties in theranostic nanogels and their profound impact on the efficacy of these multifunctional agents.

2. Fabrication of nanogels

As previously mentioned, nanogels are crosslinked soft polymeric nanostructures that do not dissolve but disperse in aqueous media. They consist of flexible hydrophilic polymer chains capable of stretching and expanding, enabling the particles to swell and retain a significant amount of water. A wide range of polymers has been utilized in the synthesis of nanogels, including natural polymers such as hyaluronic acid, chitosan, cellulose, and alginate, as well as synthetic polymers like poly(ethylene glycol) (PEG), poly(acrylic acid) (PAA), poly(lactic acid), and others. In the fabrication of nanogels, two main approaches have been widely employed: polymerization of monomers and crosslinking of pre-formed polymers (Scheme 3). The first approach often involves reverse emulsion polymerization, which relies on nanosized emulsions to determine the shape and size of nanogels.[38] Monomers within these emulsions are polymerized directly into nanogels in the presence of bifunctional monomers. While this method eliminates the need for pre-formed polymers or additional crosslinking strategies, it does require the introduction of initiators and emulsifiers to the system, which may introduce undesired toxicity concerns. The second approach for obtaining nanogels involves the crosslinking of pre-formed polymers in their nano-size forms. Within this approach, two commonly used methods to create these nano-size forms are aggregation and the nano-emulsion method.[39–42]

In the aggregation method, polymers self-assemble into nano-aggregates through physical interactions such as hydrophobicity and electrostatic interactions. Nanogels can then be prepared by crosslinking these polymeric nano-aggregates. In the nano-emulsion method, polymers are encapsulated within pre-formed nano-size emulsions, allowing for the size of these polymer clusters to be well-tuned according to the emulsion size. Once stable clusters are formed, nanogels can be produced through crosslinking, which may vary depending on the functional groups present on the polymer chains. Generally, crosslinking strategies can be categorized as chemical or physical. Chemical crosslinking involves the formation of new covalent bonds between polymers or between polymers and crosslinkers. Physical crosslinking, on the other hand, relies on physical interactions such as hydrogen bonding, electrostatic interactions, hydrophobic interactions, host–guest interactions, and chain entanglements. While chemical crosslinking results in relatively stable bonds, physical crosslinking creates loosely bonded structures. The primary motivation behind these diverse nanogel designs and synthetic approaches is to develop highly specific constructs capable of exhibiting desired behavior during transport and upon arrival at the disease site.

3. Imaging modalities in theranostic nanogels

3.1. Nanogels incorporating magnetic resonance imaging modality

MRI stands as a cornerstone in non-invasive, high-resolution imaging techniques widely employed in oncology for disease diagnostics. Despite its prowess, MRI often necessitates the

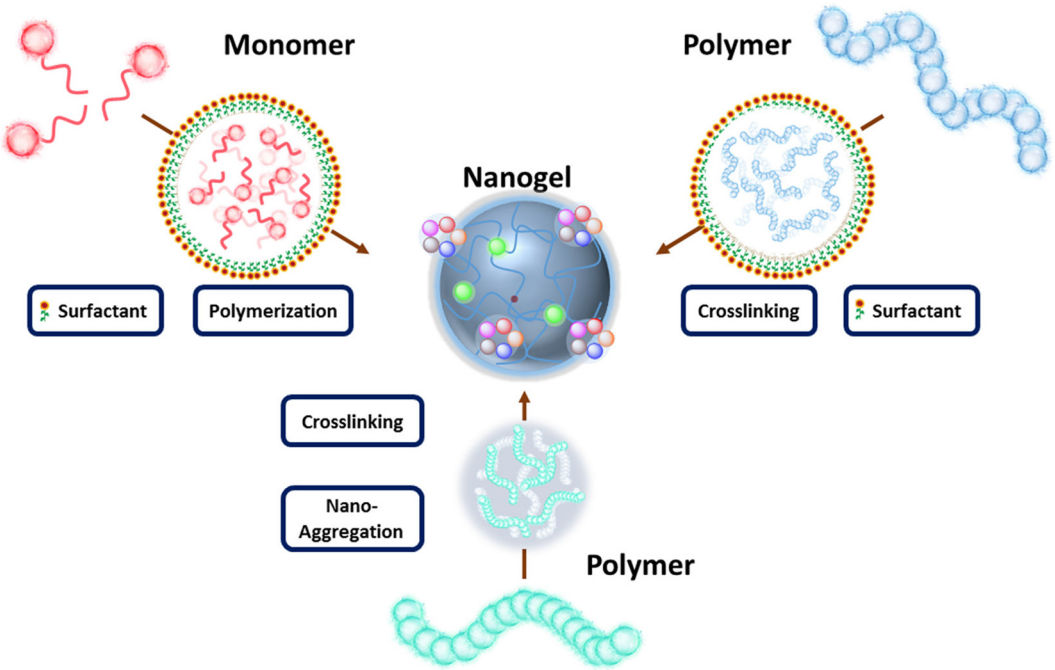

Scheme 3 A general illustration of the fabrication methods of nanogels.

use of contrast agents to enhance sensitivity.[43,44] However, achieving selective delivery of MRI contrast agents to specific tissues poses a significant challenge with most clinically utilized formulations lacking targeting capabilities. Addressing this challenge, nanogel-based MRI contrast agent formulations have emerged as a promising solution.[45,46] These formulations not only improve targeting but also increase sensitivity, offering more comprehensive insights into disease states. Efficient targeting ability is achieved through passive or active mechanisms. Passive targeting relies on nanogel size, while active targeting employs specific ligands binding to overexpressed receptors on cancer cells. The general approach involves loading nanogels with MRI contrast agents like gadolinium chelates or iron oxide nanoparticles through physical encapsulation or chemical conjugation. For instance, crosslinked nanogels with a dense inner core enable the physical encapsulation of MRI agents without leakages. A notable study by Podgórna *et al.* in 2017 demonstrated the synthesis of gadolinium alginate nanogels as personalized theranostics.[47] In this approach, aqueous solutions of gadolinium(III) chloride hexahydrate and sodium alginate were separately added to an oil phase containing surfactant to form stable microemulsions (Fig. 1a). Subsequently, the pre-formed microemulsion solutions were mixed to yield nanogels (GdNG) with diameters around 100 nm (Fig. 1b). These fabricated nanogels were further modified with polycation (chitosan) and polyanion (alginate) polymers using the layer-by-layer technique to modify surface charges. Analysis of free gadolinium content in a 2-month-old sample revealed no gadolinium leakage. Gadolinium complexes acted as positive ($T1$) contrast agents in MRI, significantly shortening the $T1$ relaxation time compared to water and gadolinium-free alginate NG (Fig. 1c). This

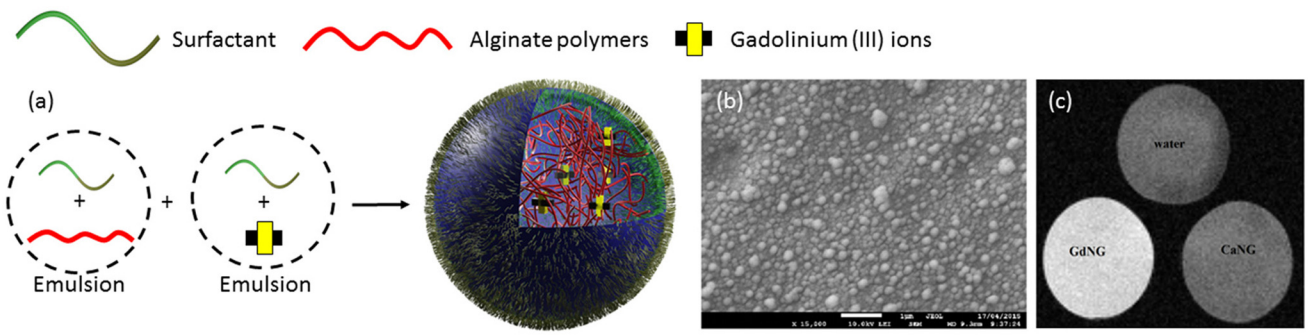

Fig. 1 (a) Fabrication of alginate nanogels crosslinked with gadolinium, (b) Cryo-SEM image of GdNG, (c) MRI results measured by $T1$ FLASH protocol of GdNG. Reproduced with permission.[47] Copyright 2017, Elsevier Inc.

study highlights the potential of nanogel-based MRI contrast agents in achieving targeted and sensitive imaging for enhanced disease diagnostics in oncology.

Magnetic iron oxide nanoparticles have emerged as another extensively investigated contrast agent for MRI, offering versatile properties and well-established synthesis protocols spanning a wide range of sizes, from a few nanometers to a hundred nanometers.[48] Both physical encapsulation and chemical conjugation to various crosslinked polymers have been successfully demonstrated in the literature.[49–54] For instance, in a study by Chen *et al.* in 2015,[55] a poly(acrylic acid) (PAA)-derived nanogel system was developed, where iron oxide (Fe_3O_4) nanoparticles (11–16 nm) were physically loaded into nanogels ranging in size from 100–120 nm. These hybrid nanogels exhibited excellent contrast in *T*2-weighted MRI, with the highest magnetization saturation of Fe_3O_4-loaded nanogels measured at 20 emu g^{-1}. Furthermore, these nanogels were able to efficiently load the chemotherapy drug doxorubicin (DOX) with a high loading capacity of 98%, and demonstrated prolonged sustained release of the drug. Importantly, nanogels modified with a cyclic arginine–glycine–aspartic acid (cRGD) targeting group exhibited selective enrichment in tumor tissue and specific binding to cancer cell membranes, as evidenced by *T*2-weighted images. Similarly, in 2013, Chiu and colleagues designed a nanogel system based on a graft copolymer containing acrylic acid, 2-methacryloylethyl acrylate, poly(ethylene glycol) (PEG), and poly(*N*-isopropyl acrylamide) (Fig. 2a).[56] Iron oxide nanoparticles and DOX were physically loaded into these hybrid nanogels for stimuli-mediated MR imaging and cancer therapy. The hybrid nanogels displayed superior transverse relaxivity (r_2) values across the entire pH range compared to iron oxide nanoparticles alone, with pH and temperature controlling the release of DOX from the nanogels. Enhanced drug release was observed at lower pH and higher temperatures, with further triggered release achieved under a high-frequency magnetic field. Notably, these hybrid nanogels demonstrated selective internalization into cells facilitated by magnetic guidance (Fig. 2b and c). These studies underscore the potential of nanogel-based systems for targeted and stimuli-responsive MRI contrast-enhanced imaging and therapy, offering promising avenues for the development of personalized cancer treatment strategies.

Approaches based on the chemical conjugation of iron oxide nanoparticles offer straightforward modifications of the nanoparticle surface, facilitating their integration into theranostic nanogels.[57,58] These modifications typically involve the use of small organic molecules and polymers, which then serve as versatile building blocks. In a notable study by Peng

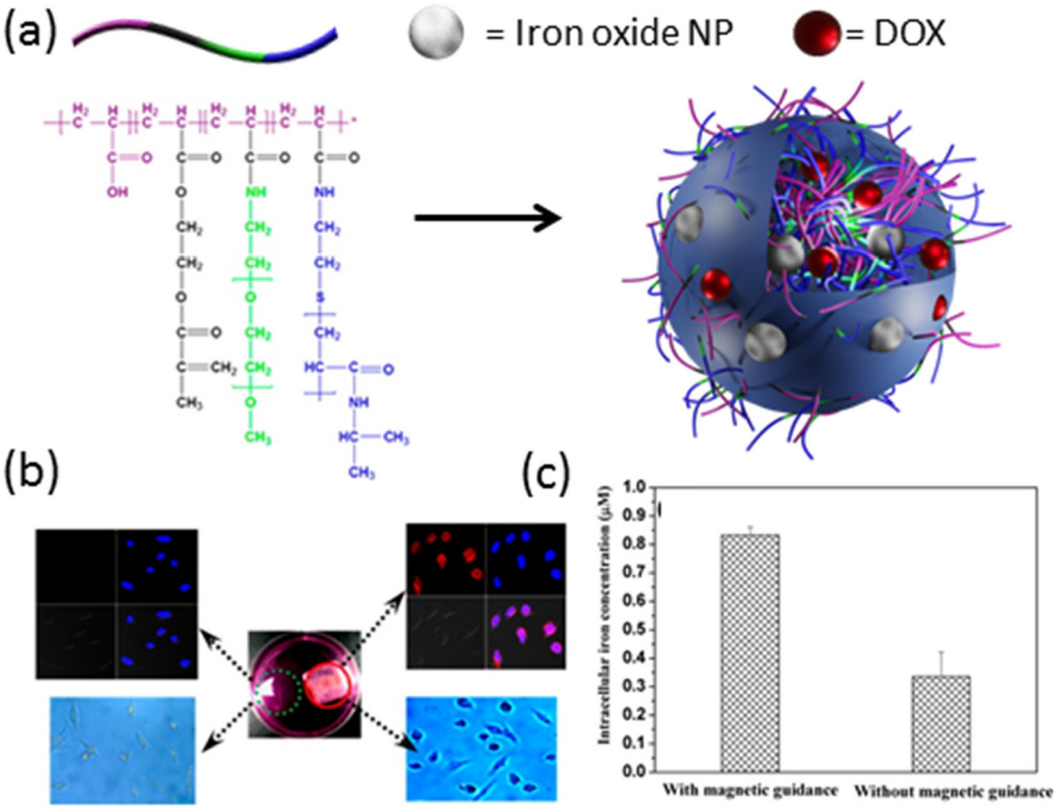

Fig. 2 (a) General representation of iron oxide nanoparticle and DOX-loaded hybrid nanogels. (b) LSCM images (top) and optical micrographs (bottom) of HeLa cells treated with DOX-loaded nanogels in the presence (red circle) and absence (green circle) of external magnetic guidance. (c) Intracellular iron concentration in the presence and absence of magnetic field. Reproduced with permission.[56] Copyright 2013, American Chemical Society.

et al. in 2019, a theranostic nanogel system was reported, wherein SPIONs were chemically conjugated to alginate and disulfide-containing alginate polymers.[59] Initially, amine-functionalized SPIONs were reacted with the alginate polymers, followed by cross-linking with $CaCl_2$ to form the nanogels (Fig. 3a). This process led to the successful incorporation of SPIONs into the nanogel matrix, resulting in a size increase (126 nm) upon loading with doxorubicin at a high loading capacity of 42 wt%. Importantly, the theranostic nanogels exhibited stimuli-responsive drug release behavior. Specifically, the release of DOX was found to gradually increase with a decrease in pH (Fig. 3b), and an increase in glutathione (GSH) concentration (Fig. 3c). These findings highlight the potential for targeted and controlled drug release in response to specific physiological stimuli, enhancing the therapeutic efficacy of the nanogels. Furthermore, the study demonstrated the utility of the nanogels for magnetic resonance imaging, with the increasing concentration of iron (Fe) in the nanogels leading to the darkening of *T*2-weighted images (Fig. 3d). Importantly, the Fe concentration was found to be linearly proportional to the relaxation rate, providing a quantitative measure of Fe concentration in the nanogels. Overall, this study showcases the versatility and potential of chemically conjugated SPIONs for the development of theranostic nanogels with integrated imaging and therapeutic capabilities. These findings pave the way for the further advancement of SPION-based nanogel systems for personalized cancer therapy and diagnosis.

In recent years, there has been growing interest in exploring drug-free approaches for cancer treatment, aiming to reduce

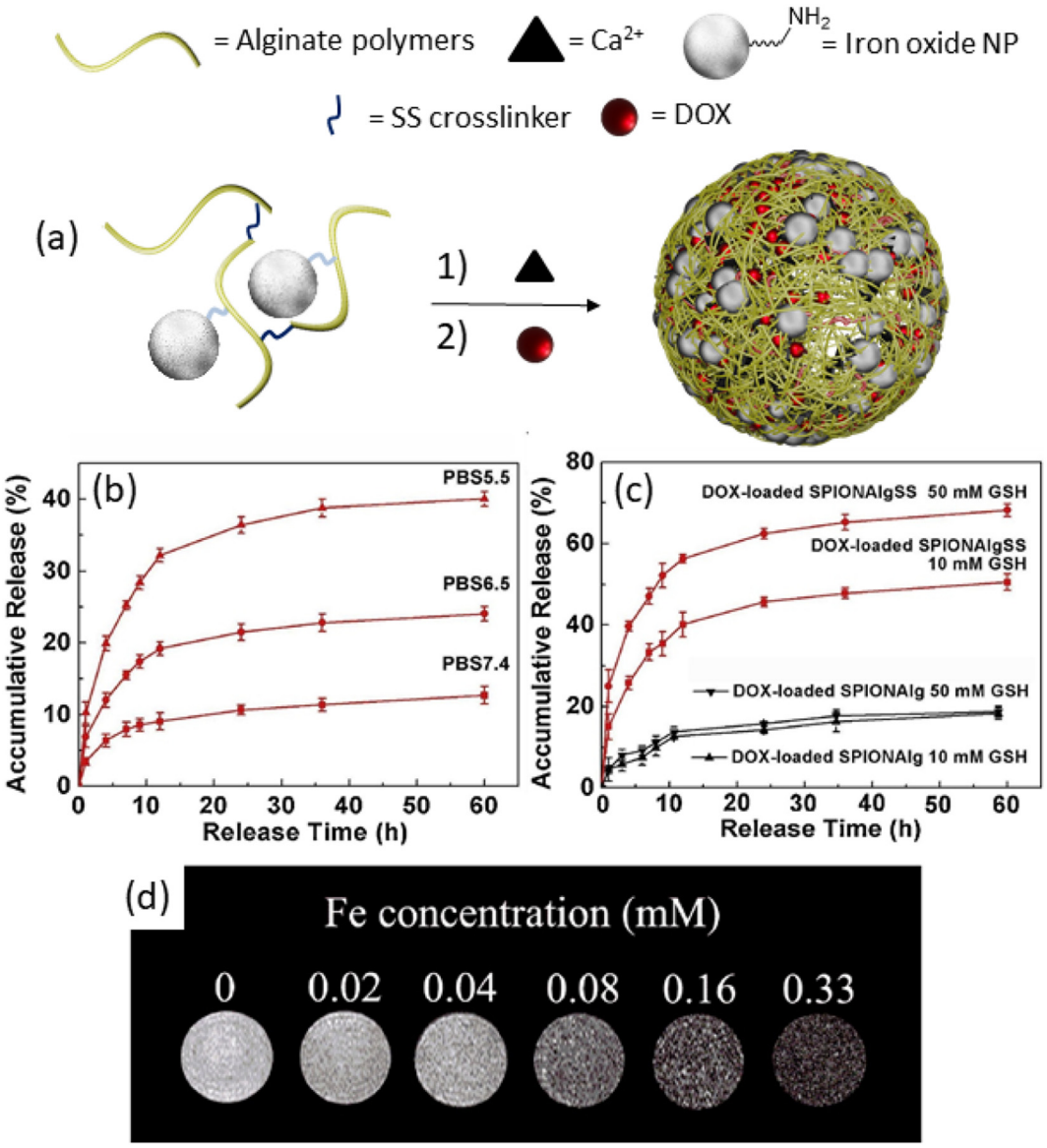

Fig. 3 (a) Synthetic of alginate nanogels, (b) release study results at different pH, and (c) GSH concentrations. (d) *T*2-Weighted MRI images of nanogels with different Fe concentrations. Reproduced with permission.[59] Copyright 2019, Elsevier Inc.

the systemic toxicity associated with traditional chemotherapeutic agents.[60–66] One such approach gaining traction involves the ablation of cancerous cells, wherein the high local temperature generated by iron oxide nanoparticles in alternating magnetic fields is utilized for magnetic hyperthermia therapy. Several studies have demonstrated the efficacy of magnetic hyperthermia therapy in selectively targeting and destroying cancer cells while minimizing damage to surrounding healthy tissues. Leveraging the heat generation and contrast-enhancing properties of iron oxide nanoparticles, Katagiri *et al.* introduced a hybrid nanogel system designed for both imaging and therapeutic applications.[67] This hybrid nanogel system, measuring 35 nm in diameter, comprises cholesterol-conjugated polysaccharide pullulan and iron oxide nanoparticles coated with oleic acid. Phantom test results revealed a dramatic increase in MR signal with the escalating concentration of hybrid nanogels, showcasing their potential as effective contrast agents for magnetic resonance imaging. Moreover, these nanogels demonstrated the capability to generate heat under alternating magnetic fields, with the temperature being modulated by adjusting the nanogel concentration and the amplitude of the applied magnetic fields. This controllable heat generation makes the hybrid nanogel system particularly promising for hyperthermia therapy, offering a cancer treatment with relatively less systemic toxicity. While a few select examples are discussed to highlight the benefits of MRI modality-based theranostic nanogels, several reports have been reported to date, and a few more examples to direct the interested reader are presented in Table 1. Overall, the development of hybrid nanogels combining MRI and therapeutic functionalities represents a promising advancement in the field of cancer therapy, opening up new avenues for personalized and precision medicine. Further research and clinical studies are warranted to validate the efficacy and safety of these innovative nanogel-based approaches in clinical settings.

3.2. Nanogels incorporating optical imaging modalities

Optical imaging modalities offer a rapid, cost-effective, and relatively sensitive approach for monitoring the localization of theranostic agents within tumor tissues. Variations in tissue characteristics such as blood volume, flow rate, or hypoxia between cancerous and healthy tissues generate endogenous optical contrast, facilitating the detection of cancer cells. However, the low sensitivity resulting from background noise poses a significant challenge in optical imaging.[68] To address this limitation, exogenous optical contrast agents have been developed to enhance sensitivity and specificity by altering the absorption, scattering, or fluorescence properties of target tissues compared to normal tissues.[69] Nanogels emerge as promising candidates for constructing optical imaging-based theranostic platforms, owing to their enhanced localization in tumor tissues through active or passive targeting mechanisms, as well as their capacity for high loading of imaging agents, thereby improving contrast efficiency.[70–77] In this section of the review, we showcase recent examples of nanogel-based theranostic agents incorporating various anticancer optical imaging agents. Additionally, we explore the influence of stimuli-responsive properties of nanogels on drug delivery and optical imaging efficiency. While select examples are discussed in detail to underscore the promising prospects of this theranostic modality, an exhaustive list of reported examples to date is provided at the conclusion of this section (Table 2).

Semiconductor quantum dots (QDs) represent light-emitting nanosized particles ranging from 2 to 10 nm, and have been extensively studied for cellular and *in vivo* imaging applications.[78] The remarkable potential of QDs in bioimaging stems from their unique optical properties, including photostability, broad absorption spectra, and well-defined narrow emission profiles.[79] Despite their superior brightness and stability against photobleaching compared to organic dyes,[80] concerns regarding QD toxicity *in vivo* have been raised, although these concerns can be addressed through appropriate surface coatings.[81–84] The exceptional optical properties of QDs render them excellent candidates for engineering theranostic nanogels with optical imaging capabilities. In a notable study in 2011, Jayakumar and coworkers developed QD-incorporated chitin theranostic nanogels.[85] These nanogels efficiently loaded bovine serum albumin (BSA) as a model protein, with the particle size of the nanogels varying proportionally to the amount of loaded BSA. Remarkably, the encapsulated BSA was completely released within 5 days under both acidic and neutral environments. Furthermore, the QD-chitin nanogels retained their luminescence for over 24 hours post-internalization, highlighting their potential for prolonged imaging applications. Moreover, the intracellular retention time of QDs was observed to be several hours, further demonstrating their

Table 1 Examples of nanogels with MRI modality employed in cancer theranostics

Imaging technique	Therapy	Cancer type	Model	Drug	Imaging agent	Stimuli-response	Ref.
MRI, US	Drug delivery	Melanoma	*In vivo*	DOX	MnO_2	Redox	45
MRI	Drug delivery	Lung cancer	*In vivo*	DOX	Fe_3O_4	Light	46
MRI	Drug delivery	—	*In vitro*	—	Rhodamine b, gadolinium	—	47
MRI	Drug delivery	—	*In vitro*	—	Fe_3O_4	Redox	50
MRI, CLSM	Drug delivery	Neuroblastoma	*In vitro*	DOX	Fe_3O_4	—	55
MRI	Drug delivery	—	*In vitro*	DOX	SPIONs	pH	57
MRI, CLSM	Drug delivery	Liver cancer	*In vitro*	DOX	SPIONs	pH, redox	59
MRI	Hyperthermia	—	*In vitro*	—	Fe_3O_4	Magnetic field	67

Abbreviations: CLSM: confocal laser scanning microscopy.

Table 2 Examples of theranostic nanogels with an optical imaging modality

Imaging technique	Therapy	Cancer type	Model	Drug	Co-molecules	Stimuli-response	Ref.
Fluorescence microscopy	Drug delivery	Breast cancer	*In vivo*	DOX	Polypyrrole	Light	71
Fluorescence microscopy	BNCT	Brain cancer	*In vivo*	^{10}B	BODIPY	—	72
PA, and NIR fluorescence imaging	Drug delivery	Liver cancer	*In vivo*	DOX	CuS	Light	75
Fluorescence microscopy	Drug delivery, photothermal therapy	Breast cancer	*In vivo*	DOX	AIE	Thermo, pH	76
Fluorescence microscopy	Drug delivery	Breast cancer	*In vitro*	Methotrexate	QD	pH	78
Fluorescence microscopy	Protein delivery	Oral, breast, prostate cancer	*In vitro*	BSA	CdTe–QDs	pH	85
CLSM	Protein delivery	—	*In vitro*	Insulin	CdTe–QDs, Fe_3O_4	—	86
MRI, fluorescence microscopy	Gene delivery	—	*In vivo*	—	Dil	Thermo	87
Fluorescence microscopy	Drug delivery	Adenocarcinoma	*In vitro*	5-FU	FITC	Light	88
Fluorescence microscopy	Drug delivery	Bone cancer	*In vitro*	DOX	G5-FI	—	90
NIR fluorescence microscopy	Photodynamic therapy	Colon cancer	*In vivo*	—	Fucoidan	Light	92
NIR fluorescence imaging	Photodynamic therapy	Fibrosarcoma	*In vivo*	—	Ce6	Redox, light	95
CLSM	Drug delivery	Lung cancer	*In vivo*	DOX	Graphene	Light, redox, pH	97
PA, thermal imaging	Photodynamic, photothermal therapy	Breast cancer	*In vivo*	—	Carbon dot	pH, redox, temperature	100
CLSM	Drug delivery	Melanoma	*In vitro*	Curcumin	FCNPs	Light, thermo	101
Fluorescence microscopy	Drug delivery	Prostate cancer	*In vitro*	DOX	RGD	pH	102
CLSM, flow cytometry	Drug delivery	Skin cancer	*In vitro*	DOX	iRGD, BSA–AuNCs	pH	103
CLSM	Drug delivery	Melanoma	*In vitro*	Dipyridamole	AgNP	pH	104
Fluorescence microscopy	Drug delivery	Breast cancer	*In vitro*	DOX	cRGD, Cy5	pH, thermo	106
NIR fluorescence	Drug delivery	Liver cancer	*In vivo*	DOX	Gold cluster	pH, redox	108
CLSM, flow cytometry	Drug delivery	Breast cancer	*In vitro*	DOX	Gelatin QDs	Redox	111
CLSM, flow cytometry	Drug delivery	Breast cancer	*In vitro*	PTX	MnO_2 FCN	Redox	112
CLSM	Drug delivery	Melanoma	*In vitro*	TMZ	Bi_2O_3 QDs	Thermo	119
CLSM	Drug delivery, photothermal therapy	Melanoma	*In vitro*	Curcumin	Ag/Au NP	Light, thermo	120
CLSM	Drug delivery	Breast cancer	*In vitro*	IAZA	FITC, RITC	Thermo	121
MRI, fluorescence microscopy	Hyperthermia	—	*In vivo*	—	SPIONs, PFBT	Magneto	124
Fluorescence microscopy	Drug delivery	Liver cancer	*In vitro*	DOX	Rhodamine B	Redox	125
CLSM	Drug delivery	Liver cancer	*In vitro*	DOX	Cy5.5	Redox, pH	126
CLSM, flow cytometry	Drug delivery	—	*In vitro*	—	CdSe–ZnS QD, RGD	Thermo, pH	127
Fluorescence microscopy	Drug delivery	Breast cancer	*In vitro*	DOX	—	Photo, pH, redox	128
CLSM	Drug delivery	Melanoma	*In vitro*	Curcumin	Carbon dot, SPIONs, carbon shell	Magneto, light	129

Abbreviations: PA: photoacustic; AIE: aggregation-induced emission; BNCT: boron neutron capture therapy; G5: generation 5 amine-terminated PAMAM dendrimers; Cy5: cyanine5 dye; TMZ: temozolomide; AgNP: Ag nanoparticle; AuNP: Au nanoparticle; RITC: rhodamine B isothiocyanate; Cy5.5: cyanine 5.5 dye; PFBT: poly(fluorene-benzothiadiazole); Dil: 1,1′-dioctadecyl-3,3,30,30-tetramethylindocarbocyanine perchlorate.

suitability for cellular imaging studies. Similarly, in 2012, Shen *et al.* utilized QDs to confer optical properties to nanogels composed of chitosan and superparamagnetic iron oxide nanoparticles.[86] They demonstrated that the photoluminescence of these nanogels increased with the incorporation of QDs-SPIONs. Leveraging the abundance of amino groups present in the chitosan polymers within the nanogel matrix, efficient loading of insulin was achieved, with the drug

primarily released within the first eight hours under acidic and physiological pH conditions. These pioneering studies underscore the potential of QD-incorporated nanogels for optical imaging applications, offering a promising avenue for the development of advanced theranostic platforms with enhanced imaging capabilities and controlled drug delivery profiles.

In addition to semiconductor quantum dots, numerous studies have delved into the utilization of fluorescent organic dyes and bioluminescent molecules as optical imaging components in theranostic nanogels.[87,88] The physical or chemical loading of these fluorescent substances into nanogels not only enhances their photostability but also significantly amplifies the imaging signal.[89] For instance, Gonçalves *et al.* pioneered the incorporation of fluorescein isothiocyanate (FI) conjugated poly(amidoamine) (PAMAM) dendrimers (G5-FI) into alginate-based nanogels (AG) to create a multifunctional drug delivery system with imaging and monitoring capabilities.[90] Through a double crosslinking strategy involving $CaCl_2$ and G5 dendrimers, the resulting nanogels exhibited enhanced stability and precise control over drug release kinetics. Remarkably, the dual crosslinked AG/G5–Dox nanogels demonstrated a significantly slower release of doxorubicin compared to AG nanogels, attributed to strong electrostatic interactions between the anionic alginate polymer and the positively charged amine-terminated dendrimers. Cell viability assays revealed that while free PAMAM dendrimers exhibited high toxicity, AG/G5 nanogels displayed minimal toxicity. Moreover, DOX-loaded AG/G5 nanogels exhibited comparable cytotoxicity to free DOX, highlighting their therapeutic efficacy. Importantly, the high fluorescence intensity exhibited by AG/G5-FI nanogels upon incubation with a human osteosarcoma cell line (CAL-72) validated their potential for cellular imaging applications. Conversely, cells exposed to G5-FI alone exhibited significant cytotoxicity and morphological alterations, underscoring the role of the nanogel matrix in mitigating the potential toxicity associated with dendrimer-based multivalent dye-conjugated fluorescent agents. In summary, this exemplary study underscores the versatility of nanogels as theranostic platforms capable of colocalizing therapeutic agents and imaging probes while mitigating potential cytotoxicity concerns. Moreover, the integration of fluorescent organic dyes which can be appropriately designed to possess specific optical properties using synthetic organic chemistry into multifunctional nanogels opens up new avenues for enhanced imaging and monitoring of therapeutic interventions in various disease settings.

Recent studies have highlighted the potential of stimuli-responsive nanogels, which can be triggered by external or internal stimuli such as pH, temperature, enzymes, sound, magnetic fields, and light, to significantly enhance their physical and chemical properties for biological applications.[91] Among these stimuli, light irradiation stands out due to its precise control parameters, including power, exposure time, and wavelength. These properties allow for the targeted manipulation of nanogels once they have accumulated at the disease site. In particular, nanogels' responsiveness to specific wavelengths of light has been exploited to induce controlled chemical and physical changes within the nanogels or their surrounding environment. This manipulation is often achieved through the incorporation of photoactive groups within the nanogel matrix, enabling the conversion of light energy into localized heat, often termed as photothermal heating. This localized heating can trigger various responses, such as the release of encapsulated therapeutic agents, changes in nanogel morphology, or alterations in the local microenvironment, all of which can be precisely regulated with spatiotemporal precision.

An alternative light-triggered approach involves harnessing the power of photosensitizers, well-studied molecules that generate reactive oxygen species (ROS) upon exposure to light of a specific wavelength. This phenomenon, known as the photodynamic effect, has been effectively employed to destroy tumors by inducing localized cytotoxicity mediated through the ROS generated at the treatment site. Among these photosensitizers, chlorin e6 (Ce6) stands out as a prominent candidate, valued not only for its photodynamic therapy (PDT) capabilities but also for its utility as an imaging agent for near-infrared (NIR) fluorescence imaging.[92] Recent advancements in nanotechnology have enabled the integration of Ce6 into nanogel formulations, offering a dual-purpose platform for both diagnosis and therapy.[93,94] In a study by Cho *et al.*, a Ce6-containing nanogel system was investigated for its potential in photodynamic therapy of cancer.[95] The nanogels, self-assembled from cysteamine-NHS-Ce6-modified fucoidan polysaccharide, exhibited a diameter of approximately 250 nm, facilitated by the hydrophobic interactions of the Ce6 moiety (Fig. 4a). An intriguing feature of this nanogel system was its inherent non-fluorescent and non-phototoxic nature, attributed to the self-quenching effect of Ce6 within the nanogel matrix. However, upon cleavage of the disulfide bonds, nanogel degradation triggered the activation of the Ce6 molecule, leading to the restoration of fluorescence and photo-toxicity. *In vivo* studies utilizing NIR fluorescence imaging demonstrated distinct differences between free Ce6-treated mice and nanogel-treated counterparts. While free Ce6-treated mice exhibited high fluorescence intensity throughout the body, nanogel-treated mice displayed significantly lower fluorescence intensity after 5 minutes post-injection (Fig. 4b). Remarkably, at 24 hours post-injection, minimal signal was detected in free Ce6-treated mice due to dye clearance, whereas nanogel-treated mice exhibited sustained fluorescence at the tumor site, indicating prolonged retention and accumulation of Ce6 within the tumor microenvironment. Further *ex vivo* NIR fluorescence imaging of tumors and major organs corroborated these findings, revealing robust fluorescence signals in nanogel-treated mice compared to their free Ce6-treated counterparts (Fig. 4c). Importantly, Ce6-incorporated nanogels demonstrated enhanced efficacy in photodynamic therapy of cancer cells *in vivo*, underscoring their potential as a promising theranostic platform.

In recent years, graphene has emerged as a versatile nanomaterial with immense potential in both therapeutic and diag-

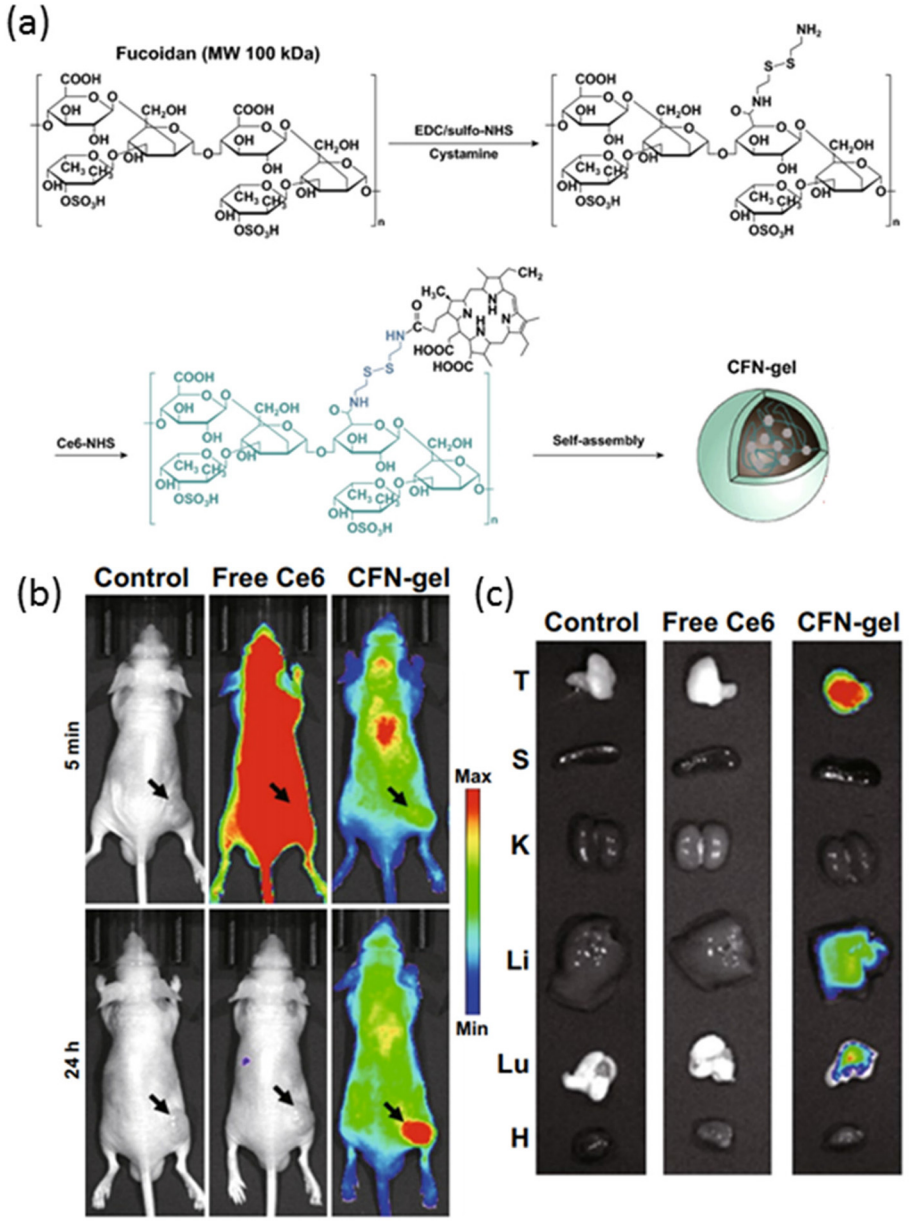

Fig. 4 (a) Fabrication of Ce6–fucoidan theranostic nanogel (CFN-gel), (b) *in vivo* NIR fluorescence images of PBS, free Ce6 and CFN-gel-treated mice, and (c) *ex vivo* NIR fluorescence images of tumors and major organs of PBS, free Ce6 and CFN-gel-treated mice. Reproduced with permission.[95] Copyright 2020, Springer.

nostic applications.[96] Its unique properties, including facile surface functionalization and efficient light absorption in the near-infrared region, make it an attractive candidate for the development of theranostic agents. Graphene can be easily oxidized to incorporate various functional groups, such as acids and alcohols, on its surface and edges, enabling the attachment of therapeutic agents through chemical conjugations. Moreover, graphene oxide exhibits strong light absorption in the NIR region, allowing it to generate heat upon irradiation, which can be utilized to trigger drug release or induce hyperthermia. Taking advantage of these properties, Lee and colleagues utilized graphene to deliver the chemotherapeutic drug doxorubicin by preparing a graphene–DOX conjugate with a pH-sensitive bond.[97] This conjugate was then loaded into hyaluronic acid nanogels, which were crosslinked through a disulfide-based crosslinker to yield a redox-, light-, and pH-responsive nanogel system (Fig. 5a). *In vitro* studies demonstrated that each trigger independently contributed to the release of DOX from the nanogels. *In vivo* photothermal imaging further revealed that the nanogels efficiently accumulated at the tumor site, where the temperature of the tumor tissue could be elevated to 52 °C after 30 minutes of irradiation with a NIR laser (670 nm, 1 W cm^{-2}). Optical imaging demonstrated an enhanced accumulation of nanogels

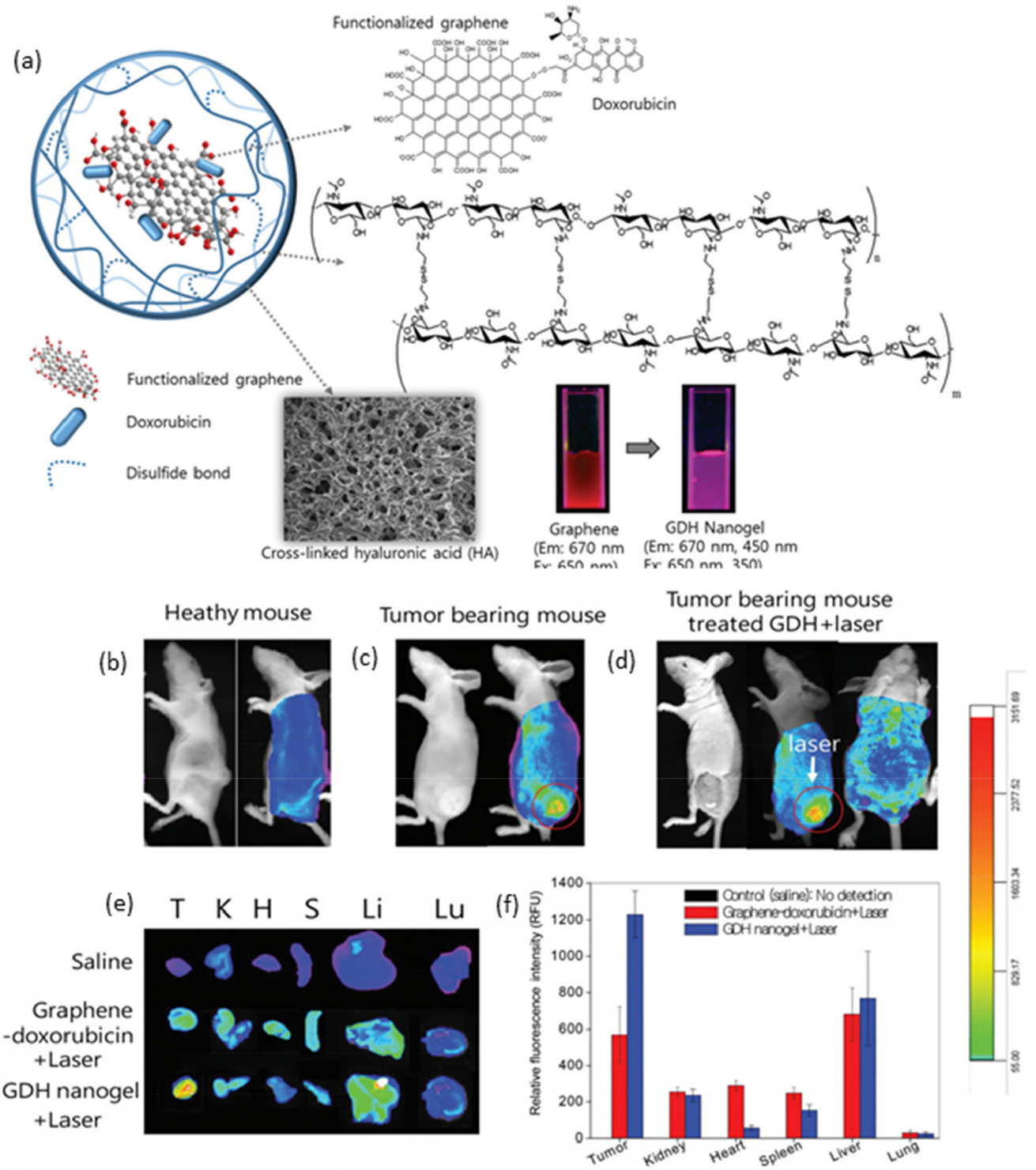

Fig. 5 (a) Schematic representation of graphene-loaded responsive nanogels; optical and fluorescence images of (b) healthy, (c) tumor-bearing mice, and (d) tumor-bearing mouse with laser irradiation; and *ex vivo* (e) fluorescence images and (f) fluorescence intensities of tumor and major organs. Reproduced with permission.[97] Copyright 2015, The Royal Society of Chemistry.

in the tumor region (Fig. 5b and c), with fluorescence intensity increasing significantly after laser irradiation (Fig. 5d). *Ex vivo* imaging of tumors and major organs corroborated these findings, showing higher fluorescence intensity in nanogel-treated tumor-bearing mice compared to those treated with saline and graphene–DOX (Fig. 5e and f). Importantly, treatment with nanogels and NIR irradiation resulted in a dramatic decrease in tumor size without a corresponding decrease in body

weight, highlighting the therapeutic efficacy and safety of this theranostic approach. These results underscore the potential of graphene-based nanogels as promising platforms for integrated cancer therapy and imaging.

Carbon-based nanoparticles, such as carbon dots and fluorescent carbon nanoparticles (FCNPs), have garnered significant attention for their potential applications in theranostics.[98] These nanoparticles possess unique photo-luminescent properties and the ability to absorb near-infrared light, which can be converted into heat,[99] rendering them promising candidates for integration into nanogel systems. Compared to graphene, carbon dots, and FCNPs offer advantages in terms of their smaller size, typically around 10 nm, making them highly suitable for incorporation into nanogels. For example, Lin and coworkers reported carbon dot integrated stimuli-responsive poly(*N*-isopropyl acrylamide) (PNIPAM-CD) hybrid nanogels for theranostic applications. These nanogels exhibit enhanced tumor accumulation, facilitated by their enlarged size, and upon exposure to deep-red-light irradiation generate heat and reactive oxygen species (ROS), enabling photothermal therapy (PTT) and photodynamic therapy (PDT). Moreover, the nanogels demonstrate pH and temperature-responsive behavior, facilitating enhanced cellular internalization. Additionally, the nanogels exhibit redox-responsive behavior, aiding in their subsequent rapid clearance from the body, which is triggered by the overexpression of glutathione (GSH) in tumor cells.[100] In another example, Wang *et al.* reported the synthesis and characterization of a nanogel system composed of poly(*N*-isopropylacrylamide-*co*-acrylamide) (PNIPAM-AAM) loaded with FCNPs for NIR-responsive drug delivery and tumor imaging.[101] In this study, FCNPs were efficiently incorporated into PNIPAM-AAM nanogels through hydrogen bonding interactions. The resulting nanogels exhibited thermo-responsive behavior, wherein an increase in temperature led to a decrease in their size. Remarkably, this decrease in size resulted in enhanced photoluminescent properties of the nanogels. Curcumin, a model drug, was successfully loaded into these nanogels, and its release was found to be temperature and light-dependent. Cell viability assays revealed that the drug-free nanogels were non-toxic, while the drug-loaded nanogels exhibited increased cytotoxicity in the presence of NIR light. These findings highlight the potential of FCNP-loaded nanogels as versatile platforms for combined drug delivery and imaging applications. Their NIR-responsive behavior, along with their biocompatibility and ability to enhance drug release under specific conditions, make them promising candidates for future theranostic applications in cancer treatment.

pH-Responsiveness represents a biological trigger that does not necessitate an external stimulus for drug release, unlike light responsiveness. In the context of diseases such as cancer, where the tumor microenvironment exhibits a lower pH compared to normal tissues, pH-sensitive chemical bonds within nanogels or between drugs and nanogels can be cleaved, triggering the release of therapeutic payloads. For instance, Gyawali *et al.* developed a pH-responsive nanogel composed of maleic acid, citric acid, lysine, and polyethylene glycol (PEG), which also exhibited photoluminescence properties.[102] The nanogel surface was functionalized with a peptide-based targeting agent, cRGD, to enhance tumor-specific accumulation. This nanogel system achieved a high loading efficiency of 92% for the anticancer drug doxorubicin at a concentration of 20 wt%. While an initial burst release was observed within the first 3 hours under both acidic and neutral pH conditions due to physical loading, subsequent pH-responsive release occurred over the following three days. In another study, Nie and colleagues developed a nanogel system composed of poly(*N*-isopropylacrylamide-*co*-acrylic acid) encapsulating gold nanoclusters (AuNCs) for the delivery of DOX.[103] Chemotherapy drug DOX was efficiently encapsulated at a concentration of 21.6 wt% with an impressive loading efficiency of 90.2%. The nanogel was functionalized with a targeting moiety, namely the N-terminal cysteine peptide tumor-homing peptide (iRGD), along with BSA–AuNCs. Drug release from the nanogel occurred to a greater extent at pH 5.2 (around 70%) compared to pH 7.4 (around 30%), indicative of pH-responsive behavior. Moreover, the red fluorescence emission from the AuNCs facilitated the monitoring of nanogel internalization *in vitro*, demonstrating enhanced uptake of targeted nanogels compared to non-targeted counterparts.

In a series of interesting studies, Zhou and colleagues pioneered the development of pH-responsive theranostic nanogels.[104] In one notable study, they engineered nanogels by incorporating cadmium selenide quantum dots (CdSe QDs) into pH and temperature-responsive hydroxypropyl cellulose-poly(acrylic acid) (HPC-PAA) matrices.[105] The hydroxyl groups present in HPC facilitated the stabilization of Cd^{2+} ions within the nanogel structure, allowing for the *in situ* synthesis of QDs. Meanwhile, PAA served as a pH-responsive component, enabling modulation of the nanogel volume in response to changes in pH levels. Temozolomide, an anticancer drug model, was physically loaded into these nanogels at a high concentration (55.4 wt%). A decrease in pH induced volume shrinkage of the nanogels, leading to an enhancement in photoluminescence (PL) intensity. Conversely, an increase in pH resulted in the disruption of hydrogen bonds within the nanogel matrix, promoting drug release. Compared to physically loaded drugs, the chemical conjugation of drugs *via* cleavable bonds significantly mitigated undesired burst release. Among the most commonly utilized pH-responsive bonds for drug conjugation are ester, carbonate, and carbamate bonds. In a recent advancement, Sanyal and co-workers designed a multifunctional nanogel system tailored for targeted drug delivery and imaging applications.[106] This nanogel platform featured maleimide, thiol, and NHS-activated carbonate functionalities, which were conjugated with a thiol-bearing cyclic peptide-based targeting ligand, a maleimide-containing near-infrared cyanine-5 dye, and an amine group-containing chemotherapeutic drug, respectively. Fluorescence imaging analysis revealed that cells treated with nanogels harboring targeting ligands exhibited heightened fluorescence intensity, indicating enhanced cellular uptake. Furthermore, the nanogels facilitated higher and sustained release of doxorubicin

through the hydrolysis of the carbamate linker, particularly under acidic conditions. These studies exemplify the versatility and potential of pH-responsive nanogels for precise and controlled drug delivery, offering opportunities for tailored theranostic applications with enhanced therapeutic efficacy and imaging capabilities. Continued advancements in this field hold promise for the development of next-generation nanogel-based theranostic platforms with improved performance and clinical translatability.

While safeguarding the encapsulated drug within the carrier during circulation to prevent systemic toxicity is crucial, achieving efficient intracellular drug release is equally important for nanoparticle efficacy. Endogenous stimuli, particularly prevalent in cancerous cells, offer a promising avenue to trigger drug release by cleaving the bonds between the drug and polymer or degrading the crosslinked nanogel network. Among these stimuli, disulfide linkages have garnered significant attention as they are redox-responsive and can be cleaved by glutathione, a tripeptide overexpressed in tumor tissues.[107] In this context, nanogels containing disulfide bonds have emerged as a promising theranostic platform.[108–110] Bhattacharya and colleagues demonstrated the impact of a reductive environment on drug release from theranostic nanogels.[111] They utilized an amphiphilic block copolymer, poly[2-(acrylamido) glucopyranose]-*b*-poly(furfuryl methacrylate), with a terminal carboxylic acid to modify gelatin quantum dots. These amphiphilic structures facilitated the formation of micellar aggregates, which were subsequently crosslinked using a disulfide-containing bismaleimide-based crosslinker through the Diels–Alder reaction, enabling simultaneous loading of doxorubicin. The cumulative release of DOX in the presence of a disulfide bond-cleaving agent and a low pH environment induced a burst release, with nearly 47% of the drug being released. Conversely, at pH 7.4 and in the absence of the cleaving agent, DOX release barely reached 20%. The green fluorescence emitted by the gelatin QDs upon excitation at 350 nm facilitated the monitoring of cellular uptake of the nanogels into the MDA-MB-231 breast cancer cell line. Choi and co-workers reported a fluorescent carbon nanogel system where drug release is redox-responsive.[112] They developed glutathione-sensitive hyaluronic acid-based fluorescent nanoparticles loaded with MnO_2 nanosheets and paclitaxel (PTX). In the reductive tumor cell microenvironment, MnO_2 was reduced to Mn^{2+}, imparting fluorescence to the fluorescent carbon nanoparticles (FCN). The MnO_2/FCN nanogel exhibited good biocompatibility and particle size of 169 nm in hydrodynamic diameter. In the absence of glutathione, the MnO_2/FCN nanoparticles remained non-fluorescent ("off" mode), while the addition of glutathione triggered the "on" mode switch for fluorescence imaging. Notably, PTX-loaded nanoparticles did not induce toxicity in a glutathione-depleted environment in a healthy MDCK cell line, whereas they exhibited high toxicity in cells incubated with 10 mM glutathione. These findings underscore the potential of redox-responsive nanogels for precise and controlled drug delivery in cancer therapy.

Thermo-responsive triggers have been employed in the development of theranostic nanogels, offering precise control over drug release and modulation of optical characteristics. A prevalent approach involves the utilization of temperature-responsive polymers, such as poly(*N*-isopropyl acrylamide) (PNIPAM), to engineer nanogels that undergo size changes in response to temperature variations.[113] This subtle alteration in temperature can induce nanogels to shrink, thereby facilitating drug release through a squeezing effect.[114,115] To introduce thermo-responsive attributes into nanogels, researchers have explored incorporating materials that can be heated upon exposure to external stimuli like light or alternating magnetic fields. Hyperthermia therapy, which utilizes high temperatures for short periods, presents a potent strategy for destroying malignant or dysfunctional tissues.[116] Moreover, temperature elevation may enhance the intensity of certain imaging agents, thereby improving resolution. Zhou and colleagues have developed several theranostic nanogels that leverage their thermo-responsive size change to modulate optical characteristics.[117,118] In one study, nanogels were synthesized by crosslinking polyvinyl alcohol (PVA) chains under γ-ray irradiation, with simultaneous *in situ* synthesis of bismuth oxide (Bi_2O_3) quantum dots for cellular imaging and termo-responsive drug delivery.[119] Interestingly, PVA nanogels without Bi_2O_3 did not exhibit any temperature-induced volume phase transition. However, temperature-dependent photoluminescence (PL) was observed for QD-containing nanogels, with PL intensity increasing at higher temperatures. In addition to influencing imaging properties, temperature variations also impacted drug release behavior. Temozolomide, an antitumor agent, was loaded into the Bi_2O_3@PVA nanogels with a loading capacity of 38.3%. Minor temperature changes had a profound effect on cumulative drug release, with a three-fold increase observed at 40 °C compared to release at 37 °C. This dual responsiveness to temperature not only enhances imaging capabilities but also fine-tunes drug release kinetics.

In another intriguing example, Zhou and colleagues developed thermo-responsive hybrid nanogels incorporating light-responsive Au/Ag nanoparticles in the core.[120] The inner shell comprised hydrophobic polystyrene, chosen for its drug-carrying capabilities, while the outer shell consisted of nonlinear hydrophilic polyethylene glycol (PEG) polymer to induce a thermo-responsive volume phase transition. This design enabled efficient dispersion of the hydrophobic drug curcumin after encapsulation, with drug release improving from 34.6% to 78.6% upon increasing the temperature from 37 to 41 °C. Additionally, nanogel-treated B16F10 cells exhibited strong fluorescence upon excitation at 405 nm, facilitating optical monitoring. In a different study, Quan *et al.* engineered fluorescein isothiocyanate-labelled (FITC) thermo-sensitive galactose-based nanogels to deliver iodoazomycin arabinofuranoside (IAZA) as a source of reactive oxygen species (ROS) for hepatocellular carcinoma treatment.[121] Above the low critical solution temperature (LCST) of the polymer, the crosslinked di (ethylene glycol) methyl ether methacrylate (DEGMA) particles became hydrophobic and deswollen, allowing for efficient

drug encapsulation. Encapsulation of IAZA significantly reduced its acute toxicity, with drug release kinetics strongly influenced by temperature. While a burst release occurred within one hour at 30 °C, the release was substantially slower at 37 °C. Confocal microscopy images of FITC-labelled nanogels demonstrated the targeting effect of the galactose moiety on asialoglycoprotein receptors (ASGPR), with high-intensity fluorescence observed in Hep-G2 human liver cancer cells, which express ASGPR. Muthu and colleagues have made important contributions to thermoresponsive theranostic nanogels.[122,123] In a recent study, they utilized a novel PEG-maleic acid-glycine-based photoluminescent co-macromer and superparamagnetic iron oxide nanoparticles along with *N*,*N*-dimethylaminoethyl methacrylate (DMEMA) to fabricate stable magneto-fluorescent nanogels (Fig. 6a).[124] Under an alternating magnetic field, SPION nanogels generated temperatures of about 60 °C for magnetic hyperthermia. *In vivo* bioimaging studies demonstrated the nanogels' strong fluorescence ability under near-infrared light with wavelengths of 675 and 710 nm, while their circulation time was approximately 48 hours, surpassing that of SPIONs alone (Fig. 6b and c). These multifunctional nanogels hold promise for theranostic applications, combining magnetic hyperthermia with optical imaging for enhanced cancer therapy.

In addition to employing single stimuli to modulate imaging and delivery properties, the use of two or more stimuli has garnered significant attention. This approach allows for the design of more sophisticated and versatile

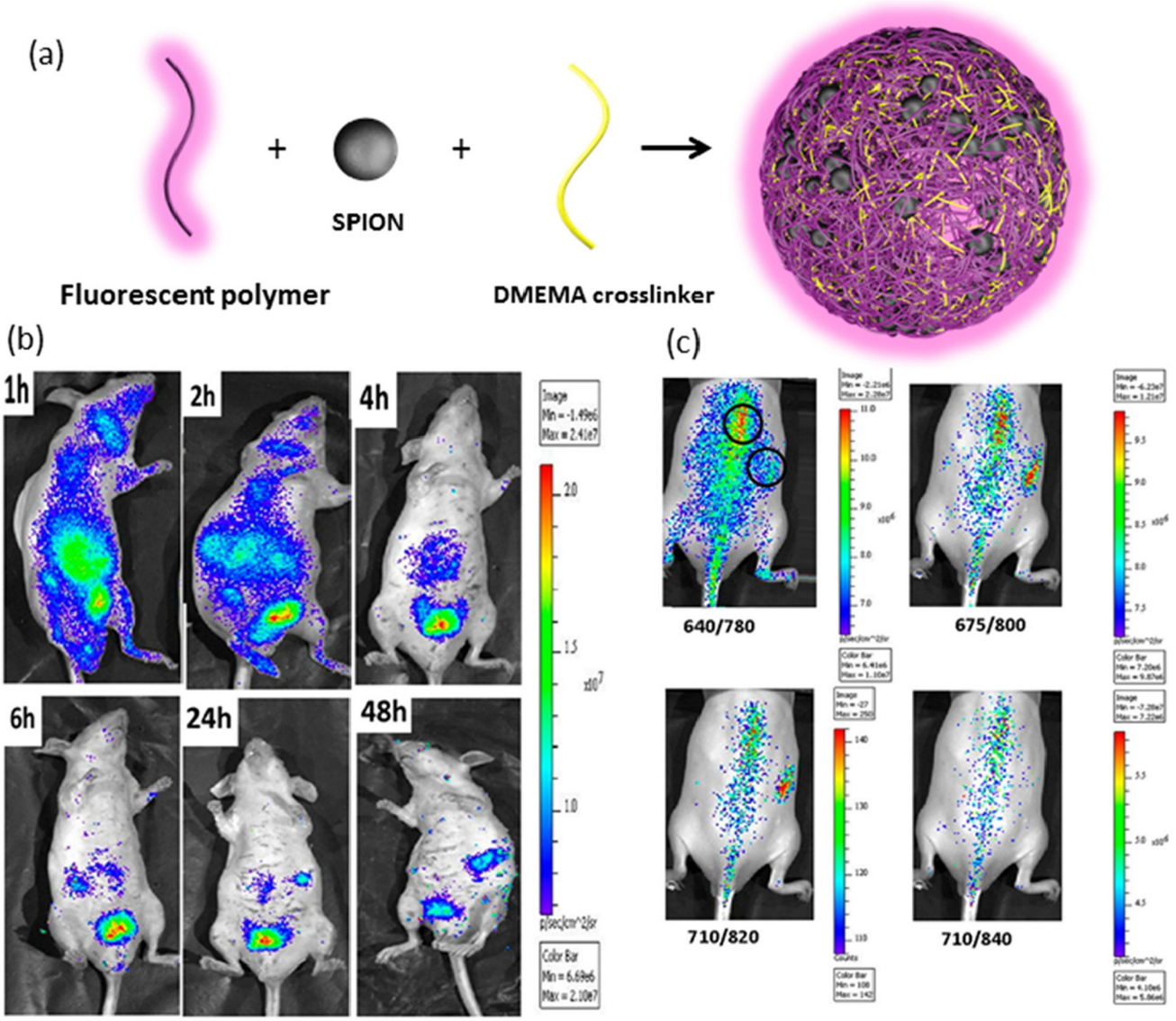

Fig. 6 (a) Schematic representation of SPION-loaded nanogels, (b) fluorescence bioimaging of intravenously injected nanogels in mice at different time points, and (c) *in vivo* biodistribution of subcutaneous injection of nanogel under different excitation wavelengths. Reproduced with permission.[124] Copyright 2019, American Chemical Society.

nanogel structures by leveraging multifunctional polymeric building blocks and diverse chemical linkages. Redox and pH-responsiveness are two commonly studied stimuli for cancer therapy. For instance, Pei *et al.* developed a dual-responsive nanogel system with imaging and targeted drug delivery capabilities.[125] In this study, oxidized alginate and folic acid (FA)

Table 3 Examples of nanogels combining photoacoustic and other imaging modalities

Imaging technique	Therapy	Cancer type	Model	Drug	Co-molecules	Stimuli-response	Ref.
PET, fluorescence imaging	Photodynamic therapy	Colon cancer	*In vivo*	—	^{124}I-labeled photosensitizer	—	147
Photoacoustic, photothermal, fluorescence imaging	Hyperthermia, drug delivery	Breast cancer	*in vivo*	Pt	MB	Light	134
Photoacoustic	Photothermal, drug delivery	Lung cancer	*In vivo*	MTX	Polypyrrole	Thermo, light	135
Photoacoustic, photothermal imaging fluorescence microscopy	Photothermal therapy	Breast cancer	*In vivo*	—	Polyaniline	—	136
Photoacoustic, MRI	Photothermal therapy	Papilloma	*In vivo*	—	DTPA-Gd, CuS	—	137
NIR II fluorescence imaging, photoacoustic imaging	Photothermal therapy	Breast cancer	*In vivo*	—	Ag_2S QDs	—	138
Gamma imaging	Drug delivery	Brain tumors	*In vivo*	5-Fluorouracil derivative	(99 m)Tc	—	146

Abbreviations: MTX: methotrexate; DTPA: diethylenetriamine pentaacetic acid; CuS: copper sulfide; Ag_2S: silver sulfide; Pt: cisplatin; MB: methylene blue.

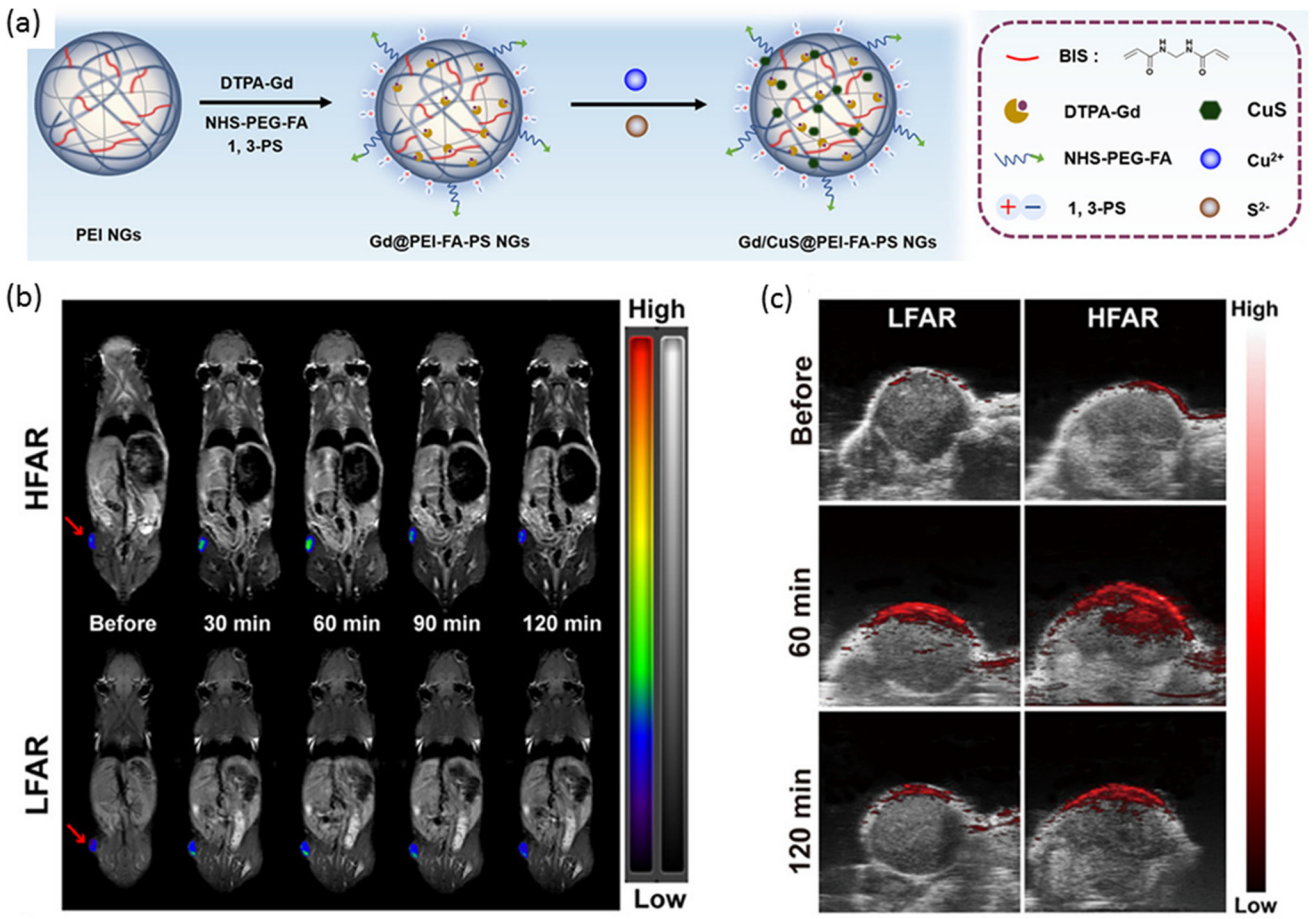

Fig. 7 (a) A general scheme of preparation of nanogels for MR and PA imaging-guided photothermal therapy. (b) *T*1-Weighted MR images and (c) PA imaging of LFAR and HFAR tumors after i.v. injection of nanogel at different time points. Reproduced with permission.[137] Copyright 2020, American Chemical Society.

and rhodamine-B terminated polyethylene glycols (PEGs) were crosslinked with cystamine. The system exploited the strong fluorescence of rhodamine at acidic pH and the targeting effect of folate groups on cancer cells. Additionally, the disulfide crosslinks and acid-labile conjugation of doxorubicin made the nanogels sensitive to the reductive tumor microenvironment. *In vitro* studies confirmed that in acidic media with the presence of glutathione (GSH), nanogels exhibited the highest release rate (up to 41%). Folate-mediated targeting enabled preferential targeting of tumor cells with overexpressed folate receptors. Nanogels loaded with DOX showed higher toxicity than free DOX in the HepG2 cell line, and their internalization into these cells was observed using fluorescence microscopy. Another example of a redox- and pH-dual responsive nanogel was reported by Jing *et al.*[126] This nanogel system comprised a crosslinked poly L-cystine core and a poly L-lysine shell synthesized from ring-opening polymerization of *N*-carboxy anhydride (NCA). The nanogel was then modified with 2,3-dimethyl maleic anhydride (DMA) and Cy5.5 NIR dye. The dual responsiveness operated in two ways: first, in a slightly acidic tumor microenvironment, hydrolysis of DMA amide occurred, resulting in a positively charged nanogel, facilitating efficient internalization. Second, disulfide bonds in the poly L-cystine core were reduced in the high concentration of GSH environment of tumor cells, promoting drug release. The cumulative drug release increased from 20.5% at pH 7.4 to 31.8% at pH 6.5, and in the presence of GSH at pH 6.5, it increased to 92.5%. DOX-loaded nanogels exhibited significantly higher toxicity than free DOX at pH 6.5 due to enhanced internalization stemming from the positively charged shell and electrostatic attraction with the cellular membrane. Fluorescence intensity was enhanced in reductive environments due to decreased aggregation with the release of the drug. Yang *et al.* reported another system utilizing temperature and pH to develop dual-responsive QD–polypeptide hybrid nanogels.[127] In this study, hydrophobic and hydrophilic dyes were loaded simultaneously as model drugs. The *in vitro* release of model drugs could be tuned by changes in temperature and pH. Moreover, by modifying polypeptide chains with an arginine–glycine–aspartic acid motif, active targeting of HeLa cells overexpressing the $\alpha_v\beta_3$ integrin receptors was confirmed through excitation of the QD and dye at different excitation wavelengths.

Chen *et al.* introduced a third stimuli-responsive element to create multi-responsive theranostic nanogels.[128] They employed poly(acrylic acid-*co*-spiropyran methacrylate) crosslinked using *N*,*N*-bis(acryloyl)cystamine, resulting in non-toxic nanogel particles with a diameter of 40–60 nm. These nanogels were responsive to UV light, redox-active thiols, and pH. Light-induced isomerization of spiropyran to its hydrophilic

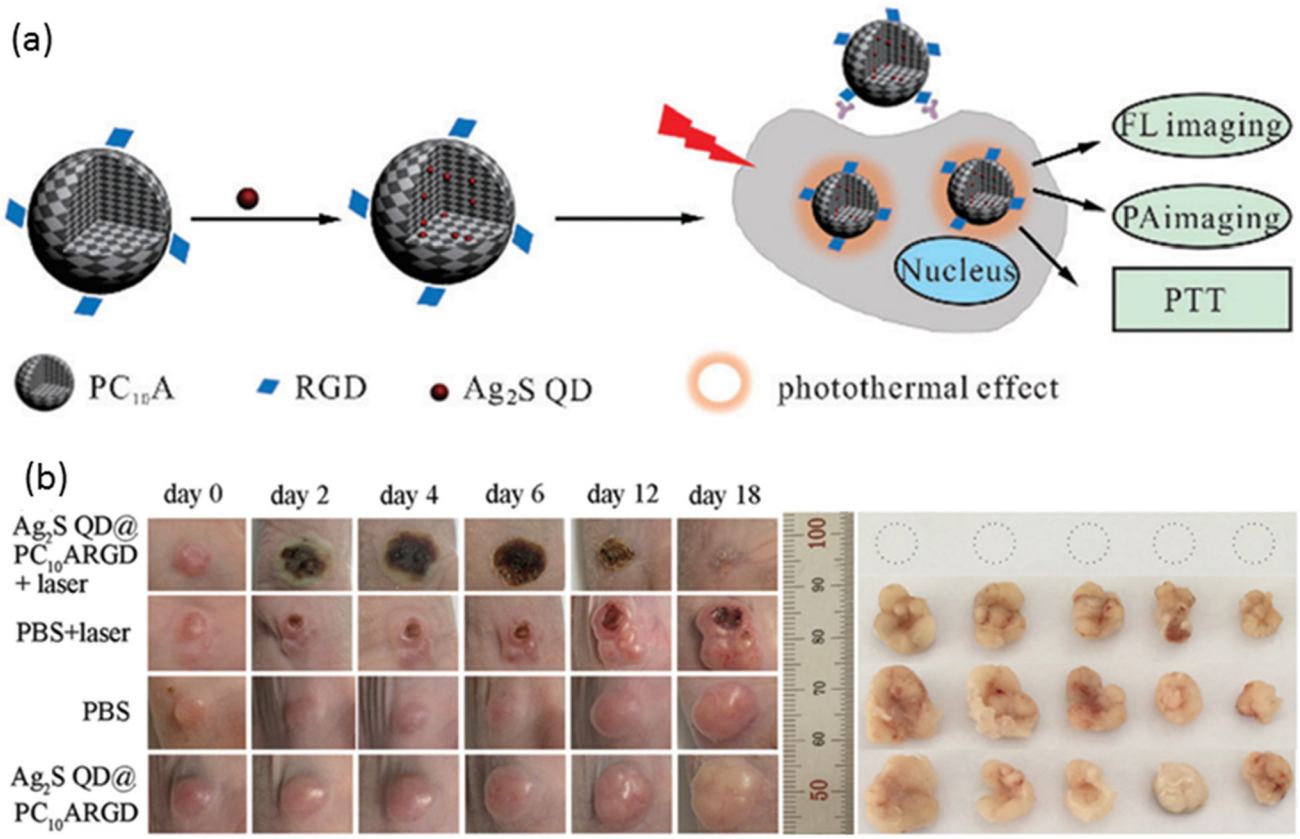

Fig. 8 (a) A general scheme for the preparation of nanogels for fluorescence and PA imaging-guided photothermal therapy. (b) The effect of PTT on tumor-bearing mice (left) and extracted tumors (right). Reproduced with permission.[138] Copyright 2018, The Royal Society of Chemistry.

form merocyanine caused swelling, accelerating drug release. Additionally, reductive environments enhanced drug release due to the scission of disulfide linkages. The fluorescence imaging ability of this system stemmed from the spiropyran group, with the merocyanine unit emitting high-intensity green light when excited at 520 nm. DOX was encapsulated into the nanogels with a loading capacity of 18%, and multi-responsiveness was confirmed with boosted cumulative release of DOX at low pH, under UV irradiation, and increased DTT concentration. Endocytosis of nanogels by MCF-7 cells was confirmed using green fluorescence under UV irradiation. Wang *et al.* reported triple-responsive nanogels *via* a core–shell approach, utilizing magnetic iron oxide nanocrystals and carbon dots for the core to achieve magneto-responsive drug release and impart optical imaging capabilities.[129] The porous carbon shell was responsible for NIR-stimulated release. These bifunctional nanoparticles were encapsulated into poly(*N*-isopropyl acrylamide-*co*-acrylamide) [poly(NiPAM-AAm)]-based shell, providing thermo-responsiveness to the nanogels. An increase in temperature resulted in smaller nanogels due to shell collapse, promoting the release of the natural anticancer drug curcumin. Below the LCST of the nanogels, low drug release was observed, but increasing the temperature from 37 °C to 41 °C doubled the release of curcumin. NIR irradiation also induced drug release due to elevated temperature. Magnetic iron oxide nanocrystals enabled a significant increase in drug release by heating after applying an alternating magnetic field. High-intensity photoluminescence was observed *in vivo* following irradiation at 405 nm due to the presence of carbon dots in the cell nucleus.

3.3. Nanogels incorporating ultrasound/photoacoustic imaging modality

Ultrasound imaging is a widely used clinical tool for detecting various benign and malignant tissues.[130,131] To enhance ultrasound signal intensity and improve the identification of fine details in tumor tissues, ultrasound imaging agents are employed.[132] Nanogels hold promise as materials for the targeted delivery of these contrast agents due to their ability to exhibit stimuli-responsive behavior and target specific tissues. Another imaging technique gaining popularity is, photoacoustic (PA) imaging, an imaging modality that merges optical and ultrasound imaging principles. The technique involves the acquisition of high-resolution images depicting tissue structures with optical contrast at depths surpassing the penetration limits of conventional optical imaging methods. In PA imaging, brief laser pulses are directed into biological tissues, where they are absorbed by intrinsic biological chromophores or external contrast agents. This absorption event induces transient thermoelastic expansion and rapid heating, generating ultrasonic waves through the PA effect. These ultrasonic waves are captured by ultrasound transducers and utilized to construct images of the tissue. PA imaging of nanogel-based systems has been used in combination with photothermal therapy and other imaging techniques (Table 3).[133,134] Calderón and colleagues have developed thermo-responsive nanogels incorporating polypyrrole (PPY), a near-infrared (NIR) transducing polymer, to facilitate the integration of photothermal and chemotherapeutic therapies, alongside photoacoustic imaging.[135] These spherical nanogels, with a hydrodynamic diameter of approximately 200 nm, demonstrated long-term stability, aqueous dispersibility, and exceptional photothermal transducing capabilities. Comprehensive *in vitro* and *in vivo* studies substantiated the nanogels' efficacy as photothermal agents and drug delivery systems, markedly inhibiting tumor growth *via* the synergistic effects of chemotherapy and photothermal treatment, while also enabling *ex vivo* biodistribution assessment through their photoacoustic contrast properties. In another example, Shi, Peng, and colleagues developed nanogels with PA imaging monitoring ability for photothermal therapy.[136] They prepared γ-polyglutamic acid nanogels loaded with the photothermal agent polyaniline (PANI) by crosslinking with cystamine dihydrochloride (cys) through 1-ethyl-3-(3-dimethyl aminopropyl) carbodiimide (EDC) coupling. These γ-PGA/Cys@PANI nanogels had an average hydrodynamic size of 689 nm and exhibited colloidal stability. The system showed a linear increase in photoacoustic signal intensity with nanogel concentration, indicating its feasibility as a contrast agent for photoacoustic imaging. Moreover, the γ-PGA/Cys@PANI nanogels demonstrated high heat generation under 785 nm laser irradiation,

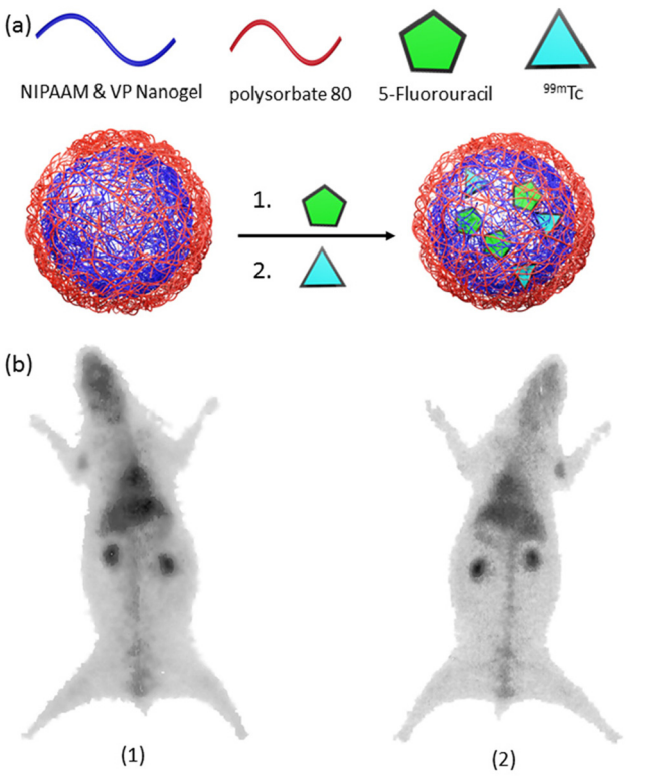

Fig. 9 (a) A general scheme for the preparation of radiolabeled-nanogels, and (b) gamma image of radiolabeled-nanogel injected rabbit after 1 h. post-injection. Reproduced with permission.[146] Copyright 2006, Taylor and Francis.

making them promising for photothermal therapy. *In vivo* experiments showed a 6-fold increase in photoacoustic signal intensity at the tumor site 30 minutes after injection, and laser irradiation for 2.5 minutes resulted in a temperature increase of 20.7 °C. Treatment with the γ-PGA/Cys@PANI nanogels followed by laser irradiation (785 nm) improved the survival rate of 4T1 tumor-bearing mice compared to control groups.

In a separate investigation, Shi, Shen, and colleagues devised a nanogel platform not only to enhance PA imaging but also MRI response, while simultaneously preserving photothermal properties for photothermal therapy (PTT).[137] The approach involved synthesizing polyethyleneimine (PEI) nanogels and functionalizing their surface with Gd(III) chelates to confer MRI contrast (Fig. 7a). Subsequent attachment of folic acid targeting ligands facilitated specific recognition of folate receptor (FAR)-expressing tumors, while modification with 1,3-propanesultone (1,3-PS) endowed the nanogels with a zwitterionic form, resulting in Gd@PEI-FA-PS nanogels. To further augment the system with PA contrast and PTT capabilities, a photothermal agent, copper sulfide (CuS), was encapsulated within the nanogels. The resulting Gd/CuS@PEI-FA-PS nanogels exhibited a diameter of 258.5 nm in the swollen state, with negligible leakage of Gd and CuS observed after 7 days. The PA and *T*1-weighted MRI signal intensities were found to be directly proportional to the concentration of the nanogels. The specificity of the FA targeting group was evaluated using both high and low-level FAR-expressing KB cell lines (KB-HFAR and KB-LFAR), revealing a 2-fold increase in cellular uptake by the high-level FAR-expressing KB cells (KB-HFAR). Laser irradiation of KB cells treated with Gd/CuS@PEI-FA-PS nanogels resulted in a significant decrease in cell viability. *In vivo* experiments demonstrated a time-dependent increase in *T*1-weighted MRI intensity post-injection, peaking after 60 minutes (Fig. 7b). PA imaging clearly delineated differences in nanogel accumulation in tumors between LFAR and HFAR-expressing cells (Fig. 7c). Furthermore, laser irradiation following intravenous injection of Gd/CuS@PEI-FA-PS nanogels induced a substantial local temperature increase in KB-HFAR tumors. Photothermal treatments validated the high efficiency of the PTT-Gd/CuS@PEI-FA-PS nanogel combination, resulting in complete tumor eradication after 8 days without observed relapse in tumor-bearing mice.

Liu, Zhao, and coworkers devised a multifunctional nanogel system featuring a synthetic polypeptide-based nanogel conjugated with RGD, with the nanogels loaded with Ag_2S QDs to confer distinctive photothermal and imaging

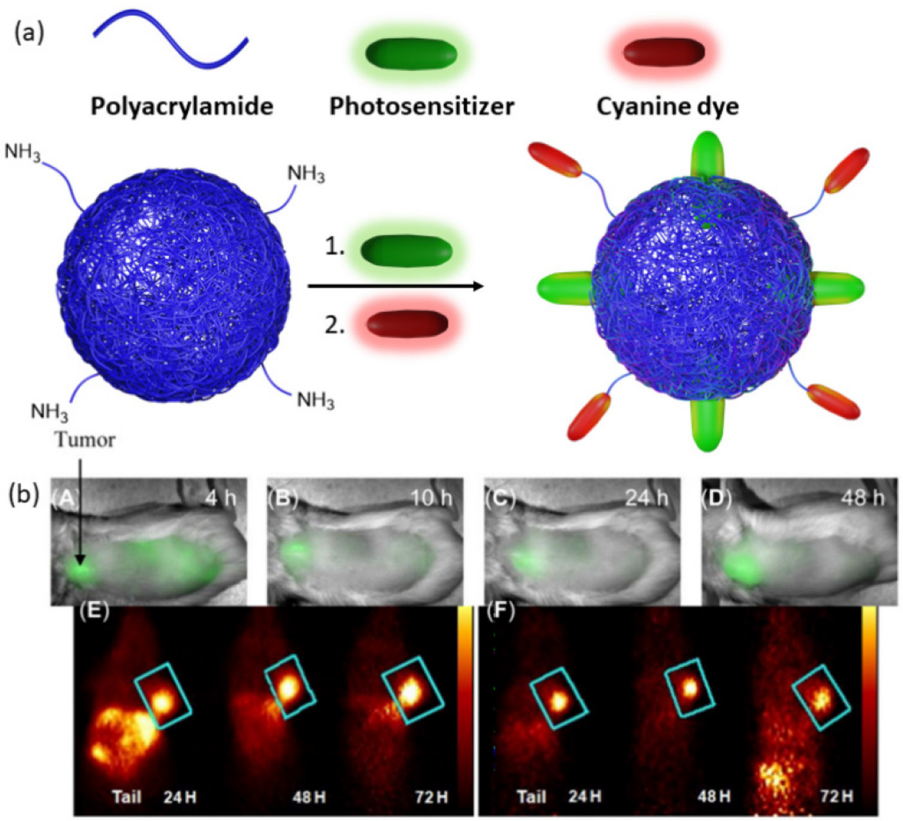

Fig. 10 (a) Representation of photosensitizer loaded, cyanine dye conjugated nanoparticles. (b) Whole-body near-infrared fluorescence imaging of nanoparticles, (A–D) 4, 10, 24, and 48 h post-injection. (E) PET imaging of cyanine dye and photosensitizer containing nanogel. (F) PET imaging of a combination of cyanine dye-containing nanogel and photosensitizer-containing nanogel. Reproduced with permission.[147] Copyright 2014, Ivyspring International Publisher.

capabilities (Fig. 8a).[138] Upon NIR laser irradiation, these nanogels exhibited a temperature increase contingent upon the concentration of Ag_2S QDs, whereas no temperature variation was observed in the absence of Ag_2S QDs. The targeting efficacy of the nanogels was validated using HeLa cells and the MCF-7 cell line, with high expression and low expression, respectively, of the $\alpha_v\beta_3$ integrin receptor. Robust fluorescence and PA intensity signals were detected in HeLa cells, indicating efficient nanogel endocytosis. PTT was administered to tumor-bearing mice treated with the nanogels, resulting in a tumor site temperature elevation of up to 60.7 °C, thereby achieving tumor suppression (Fig. 8b).

3.4. Nanogels incorporating PET/SPECT imaging modality

The significance of PET in oncology over the past decade cannot be overstated, given its high reliability in assessing cancer status and distinguishing between benign and malignant primary tumors.[139] Similarly, SPECT has made invaluable contributions to clinical oncology, offering superior diagnostic accuracy compared to other imaging modalities in tumor characterization.[140] Despite the myriad nanogel systems in conjunction with PET/SPECT imaging,[141–143] studies involving theranostic nanogels remain scarce (Table 3).[144,145] A noteworthy example of radiolabeling nanogels was reported by Soni *et al.*[146] In their study, *N*,*N*-methylene bisacrylamide (MBA) was employed to crosslink *N*-isopropyl acrylamide (NIPAAM) and *N*-vinylpyrrolidone, yielding a nanogel platform designed for delivering *N*-hexylcarbamoyl-5-fluorouracil (HCFU) to brain tissue (Fig. 9a). These nanogels were coated with polysorbate 80 to facilitate penetration of the blood–brain barrier and labeled with 99mTc to confer 2D gamma scintigraphy imaging capability. The polysorbate 80-coated nanogels exhibited a size of 50 nm, with an HCFU loading efficiency of 80%. It was reported that polysorbate 80 coating prolonged the nanogels' residence time in the blood and enhanced accumulation in brain tissue. Gamma imaging of coated and HCFU-loaded nanogels in rabbits revealed increased drug uptake in brain tissue with polysorbate coating, nearly tripling the uptake compared to uncoated nanogels (Fig. 9b).

Another theranostic nanoplatform for PET/fluorescence imaging techniques was reported by Pandey and coworkers.[147] In their study, they aimed to enhance the pharmacokinetic profile of a radioactive ^{124}I-labeled photosensitizer by encapsulating it within polyacrylamide-based nanoparticles (Fig. 10a). This nanoparticle/photosensitizer formulation exhibited improved tumor uptake while reducing accumulation in the spleen and liver. Furthermore, by conjugating cyanine dye, the combined nanoparticle/photosensitizer formulation displayed enhanced tumor imaging capabilities, combining PET and near-infrared fluorescence modalities. These advancements were validated in BALB/c mice bearing colon26 tumors (Fig. 10b). The results underscored the superior performance of the new combination compared to a free, non-labeled photosensitizer, particularly in achieving long-term cure through PDT.

4. Conclusion

From the examples highlighted in the preceding sections, theranostic nanogels emerge as a compelling platform for drug delivery and diagnostics, offering a transformative potential in healthcare. However, their transition from laboratory innovation to clinical practice encounters formidable hurdles. Indeed, these intelligent soft nanomaterials hold tremendous promise in reshaping medical approaches, enabling precise disease detection, monitoring, and targeted therapy. Their dynamic responsiveness to stimuli, coupled with multifunctionality, endows them with unprecedented capabilities to navigate biological complexities, delivering therapeutics while concurrently offering insights through advanced imaging modalities. Yet, key challenges loom, particularly concerning the translation of nanogels from experimental to clinical realms. Addressing these hurdles demands comprehensive preclinical evaluations to ascertain safety, immunogenicity, clearance, and long-term effects crucial for clinical acceptance. Overcoming challenges in scale-up and reproducible production to meet regulatory standards is essential, given the complex functionalization of nanogels with multiple agents. Moreover, ensuring effective targeting in human studies and maintaining stability for market viability are critical concerns for both manufacturers and clinicians. Ultimately, clinical validation will drive progress in theranostic nanogels. Collaborative efforts among researchers, clinicians, industry players, and regulatory bodies are imperative to surmount technical, regulatory, and economic barriers, facilitating successful translation into clinical practice. Despite the challenges, the potential benefits of theranostic nanogels in improving treatment outcomes and patient care underscore the significance of continued research and development efforts. As we navigate these challenges, the promise of theranostic nanogels in revolutionizing healthcare remains captivating, offering hope for enhanced therapies and improved patient outcomes.

Author contributions

The manuscript was written through the contributions of all authors. IA and YA did the literature survey and composed the initial draft, RS and AS did the final writing and editing. All authors have approved to the final version of the manuscript.

Data availability

No new primary research results have been included and no new data were generated or analyzed as part of this review entitled 'Theranostic Nanogels: Multifunctional Agents for Simultaneous Therapeutic Delivery and Diagnostic Imaging'.

Conflicts of interest

The authors declare no competing financial interest.

References

1 S. N. Bhatia, X. Chen, M. A. Dobrovolskaia and T. Lammers, *Nat. Rev. Cancer*, 2022, **22**, 550–556.
2 M. A. Raheem, M. A. Rahim, I. Gul, X. Zhong, C. Xiao, H. Zhang, J. Wei, Q. He, M. Hassan, C. Y. Zhang, D. Yu, V. Pandey, K. Du, R. Wang, S. Han, Y. Han and P. Qin, *OpenNano*, 2023, **12**, 100152.
3 T. Lammers, S. Aime, W. E. Hennink, G. Storm and F. Kiessling, *Acc. Chem. Res.*, 2011, **44**, 1029–1038.
4 G. Nabil, K. Bhise, S. Sau, M. Atef, H. A. El-Banna and A. K. Iyer, *Drug Discovery Today*, 2019, **24**, 462–491.
5 H. Maeda, J. Wu, T. Sawa, Y. Matsumura and K. Hori, *J. Controlled Release*, 2000, **65**, 271–284.
6 S. Guo and L. Huang, *Biotechnol. Adv.*, 2014, **32**, 778–788.
7 R. S. Kadam, D. W. A. Bourne and U. B. Kompella, *Drug Metab. Dispos.*, 2012, **40**, 1380–1388.
8 A. Nitti, R. Carfora, G. Assanelli, M. Notari and D. Pasini, *ACS Appl. Nano Mater.*, 2022, **5**, 13985–13997.
9 J. Song, X. Yang, Z. Yang, L. Lin, Y. Liu, Z. Zhou, Z. Shen, G. Yu, Y. Dai, O. Jacobson, J. Munasinghe, B. Yung, G. J. Teng and X. Chen, *ACS Nano*, 2017, **11**, 6102–6113.
10 Y. Guo, W. Chen, W. Wang, J. Shen, R. Guo, F. Gong, S. Lin, D. Cheng, G. Chen and X. Shuai, *ACS Nano*, 2012, **6**, 10646–10657.
11 A. Paul, A. Jana, S. Karthik, M. Bera, Y. Zhao and N. D. P. Singh, *J. Mater. Chem. B*, 2016, **4**, 521–528.
12 P. Mohan and N. Rapoport, *Mol. Pharmaceutics*, 2010, **7**, 1959–1973.
13 C. Zavaleta, B. Goins, A. Bao, L. McManus, C. A. McMahan and W. Phillips, *J. Drug Targeting*, 2008, **16**, 626–637.
14 B. Fadeel, *Front. Immunol.*, 2019, **10**, 133.
15 M. Chan and A. Almutairi, *Mater. Horiz.*, 2016, **3**, 21–40.
16 H. Wang, Q. Chen and S. Zhou, *Chem. Soc. Rev.*, 2018, **47**, 4198–4232.
17 A. Vashist, A. Kaushik, A. Vashist, J. Bala, R. Nikkhah-Moshaie, V. Sagar and M. Nair, *Drug Discovery Today*, 2018, **23**, 1436–1443.
18 E. Mauri, G. Perale and F. Rossi, *ACS Appl. Nano Mater.*, 2018, **1**, 6525–6541.
19 P. Saha, R. Ganguly, X. Li, R. Das, N. K. Singha and A. Pich, *Macromol. Rapid Commun.*, 2021, **42**, 2100112.
20 N. K. Preman, S. Jain and R. P. Johnson, *ACS Omega*, 2021, **6**, 5075–5090.
21 X. Zhang, S. Malhotra, M. Molina and R. Haag, *Chem. Soc. Rev.*, 2015, **44**, 1948–1973.
22 Y. Jiang, J. Chen, C. Deng, E. J. Suuronen and Z. Zhong, *Biomaterials*, 2014, **35**, 4969–4985.
23 J. K. Oh, R. Drumright, D. J. Siegwart and K. Matyjaszewski, *Prog. Polym. Sci.*, 2008, **33**, 448–477.
24 I. Neamtu, A. G. Rusu, A. Diaconu, L. E. Nita and A. P. Chiriac, *Drug Delivery*, 2017, **24**, 539–557.
25 E. Mauri, G. Perale and F. Rossi, *ACS Appl. Nano Mater.*, 2018, **1**, 6525–6541.
26 Y. L. Colson and M. W. Grinstaff, *Adv. Mater.*, 2012, **24**, 3878–3886.
27 N. K. Preman, R. R. Barki, A. Vijayan, S. G. Sanjeeva and R. P. Johnson, *Eur. J. Pharm. Biopharm.*, 2020, **157**, 121–153.
28 S. S. Das, P. Bharadwaj, M. Bilal, M. Barani, A. Rahdar, P. Taboada, S. Bungau and G. Z. Kyzas, *Polymers*, 2020, **12**, 1397.
29 L. Beria, T. N. Gevrek, A. Erdog, R. Sanyal, D. Pasini and A. Sanyal, *Biomater. Sci.*, 2013, **2**, 67–75.
30 D. Puppi, C. Migone, A. Morelli, C. Bartoli, M. Gazzarri, D. Pasini and F. Chiellini, *J. Bioact. Compat. Polym.*, 2016, **31**, 531–549.
31 M. Molina, M. Asadian-Birjand, J. Balach, J. Bergueiro, E. Miceli and M. Calderón, *Chem. Soc. Rev.*, 2015, **44**, 6161–6186.
32 A. Díaz-Moscoso, *Int. J. Med. Biomed. Res.*, 2012, **1**, 12–23.
33 P. L. Latreille, V. Adibnia, A. Nour, J. M. Rabanel, A. Lalloz, J. Arlt, W. C. K. Poon, P. Hildgen, V. A. Martinez and X. Banquy, *Nat. Commun.*, 2019, **10**, 1–8.
34 F. Rancan, M. Asadian-Birjand, S. Dogan, C. Graf, L. Cuellar, S. Lommatzsch, U. Blume-Peytavi, M. Calderón and A. Vogt, *J. Controlled Release*, 2016, **228**, 159–169.
35 A. C. Anselmo, M. Zhang, S. Kumar, D. R. Vogus, S. Menegatti, M. E. Helgeson and S. Mitragotri, *ACS Nano*, 2015, **9**, 3169–3177.
36 A. C. Anselmo and S. Mitragotri, *Adv. Drug Delivery Rev.*, 2017, **108**, 51–67.
37 S. Wilhelm, A. J. Tavares, Q. Dai, S. Ohta, J. Audet, H. F. Dvorak and W. C. W. Chan, *Nat. Rev. Mater.*, 2016, **1**, 1–12.
38 K. O. Jung, D. J. Siegwart, H. Il Lee, G. Sherwood, L. Peteanu, J. O. Hollinger, K. Kataoka and K. Matyjaszewski, *J. Am. Chem. Soc.*, 2007, **129**, 5939–5945.
39 J. H. Ryu, R. T. Chacko, S. Jiwpanich, S. Bickerton, R. P. Babu and S. Thayumanavan, *J. Am. Chem. Soc.*, 2010, **132**, 17227–17235.
40 N. M. Matsumoto, D. C. González-Toro, R. T. Chacko, H. D. Maynard and S. Thayumanavan, *Polym. Chem.*, 2013, **4**, 2464–2469.
41 B. Aktan, L. Chambre, R. Sanyal and A. Sanyal, *Biomacromolecules*, 2017, **18**, 490–497.
42 L. Chambre, W. S. Saw, G. Ekineker, L. V. Kiew, W. Y. Chong, H. B. Lee, L. Y. Chung, Y. Bretonnière, F. Dumoulin and A. Sanyal, *Bioconjugate Chem.*, 2018, **29**, 4149–4159.
43 S. Corradini, F. Alongi, N. Andratschke, C. Belka, L. Boldrini, F. Cellini, J. Debus, M. Guckenberger, J. Hörner-Rieber, F. J. Lagerwaard, R. Mazzola, M. A. Palacios, M. E. P. Philippens, C. P. J. Raaijmakers, C. H. J. Terhaard, V. Valentini and M. Niyazi, *Radiat. Oncol.*, 2019, **14**, 92.
44 J. Wahsner, E. M. Gale, A. Rodríguez-Rodríguez and P. Caravan, *Chem. Rev.*, 2018, **119**, 957–1057.
45 F. Xu, J. Zhu, L. Lin, C. Zhang, W. Sun, Y. Fan, F. Yin, J. C. M. van Hest, H. Wang, L. Du and X. Shi, *Theranostics*, 2020, **10**, 4349–4358.

46 C. Biglione, J. Bergueiro, S. Wedepohl, B. Klemke, M. C. Strumia and M. Calderón, *Nanoscale*, 2020, **12**, 21635–21646.
47 K. Podgórna, K. Szczepanowicz, M. Piotrowski, M. Gajdošová, F. Štěpánek and P. Warszyński, *Colloids Surf., B*, 2017, **153**, 183–189.
48 Z. R. Stephen, F. M. Kievit and M. Zhang, *Mater. Today*, 2011, **14**, 330–338.
49 X. Chen, X. Guo, S. Hao, T. Yang and J. Wang, *Arabian J. Chem.*, 2022, **15**, 103748.
50 L. Zhang, H. Xue, Z. Cao, A. Keefe, J. Wang and S. Jiang, *Biomaterials*, 2011, **32**, 4604–4608.
51 Y. Zou, D. Li, Y. Wang, Z. Ouyang, Y. Peng, H. Tomás, J. Xia, J. Rodrigues, M. Shen and X. Shi, *Bioconjugate Chem.*, 2020, **31**, 907–915.
52 M. K. Jaiswal, M. De, S. S. Chou, S. Vasavada, R. Bleher, P. V. Prasad, D. Bahadur and V. P. Dravid, *ACS Appl. Mater. Interfaces*, 2014, **6**, 6237–6247.
53 W. Sun, J. Yang, J. Zhu, Y. Zhou, J. Li, X. Zhu, M. Shen, G. Zhang and X. Shi, *Biomater. Sci.*, 2016, **4**, 1422–1430.
54 V. Nandwana, S. R. Ryoo, T. Zheng, M. M. You and V. P. Dravid, *ACS Biomater. Sci. Eng.*, 2019, **5**, 3049–3059.
55 Y. Chen, J. Nan, Y. Lu, C. Wang, F. Chu and Z. Gu, *J. Biomed. Nanotechnol.*, 2015, **11**, 771–779.
56 W. H. Chiang, V. T. Ho, H. H. Chen, W. C. Huang, Y. F. Huang, S. C. Lin, C. S. Chern and H. C. Chiu, *Langmuir*, 2013, **29**, 6434–6443.
57 N. Dezham, A. Zarrin, E. Parhizkar, P. Ghasemiyeh and S. M. Samani, *BioNanoScience*, 2024, 1–14.
58 N. Zhu, H. Ji, P. Yu, J. Niu, M. Farooq, M. Akram, I. Udego, H. Li and X. Niu, *Nanomaterials*, 2018, **8**, 810.
59 N. Peng, X. Ding, Z. Wang, Y. Cheng, Z. Gong, X. Xu, X. Gao, Q. Cai, S. Huang and Y. Liu, *Carbohydr. Polym.*, 2019, **204**, 32–41.
60 K. Mahmoudi, A. Bouras, D. Bozec, R. Ivkov and C. Hadjipanayis, *Int. J. Hyperthermia*, 2018, **34**, 1316–1328.
61 Y. Cheng, S. Weng, L. Yu, N. Zhu, M. Yang and Y. Yuan, *Integr. Cancer Ther.*, 2019, **18**, 1534735419876345.
62 S. Jha, P. K. Sharma and R. Malviya, *Achiev. Life Sci.*, 2016, **10**, 161–167.
63 J. Beik, Z. Abed, F. S. Ghoreishi, S. Hosseini-Nami, S. Mehrzadi, A. Shakeri-Zadeh and S. K. Kamrava, *J. Controlled Release*, 2016, **235**, 205–221.
64 G. Fiorentini, D. Sarti, C. D. Gadaleta, M. Ballerini, C. Fiorentini, T. Garfagno, G. Ranieri and S. Guadagni, *Integr. Cancer Ther.*, 2020, **19**, 1534735420932648.
65 J. Jose, R. Kumar, S. Harilal, G. E. Mathew, D. G. T. Parambi, A. Prabhu, M. S. Uddin, L. Aleya, H. Kim and B. Mathew, *Environ. Sci. Pollut. Res.*, 2020, **27**, 19214–19225.
66 S. K. Sharma, N. Shrivastava, F. Rossi, L. D. Tung and N. T. K. Thanh, *Nano Today*, 2019, **29**, 100795.
67 K. Katagiri, K. Ohta, K. Sako, K. Inumaru, K. Hayashi, Y. Sasaki and K. Akiyoshi, *ChemPlusChem*, 2014, **79**, 1631–1637.
68 C. G. Hadjipanayis, H. Jiang, D. W. Roberts and L. Yang, *Semin. Oncol.*, 2011, **38**, 109–118.
69 K. Licha, *Top. Curr. Chem.*, 2002, 1–29.
70 A. Vashist, A. D. Raymond, P. Chapagain, A. Vashist, A. Y. Arias, N. Kolishetti and M. Nair, *J. Neurovirol.*, 2023, **29**, 252–257.
71 T. Xiao, W. Hu, Y. Fan, M. Shen and X. Shi, *Theranostics*, 2021, **11**, 7057–7071.
72 S. Coninx, G. Kalot, A. Godard, E. Bodio, C. Goze, L. Sancey and R. Auzély-Velty, *Int. J. Pharm.: X*, 2022, **4**, 100134.
73 H. Cai and P. Yao, *Nanoscale*, 2013, **5**, 2892–2900.
74 Y. Chen, X. Zheng, X. Wang, C. Wang, Y. Ding and X. Jiang, *ACS Macro Lett.*, 2014, **3**, 74–76.
75 Z. Zhang, X. Zhang, Y. Ding, P. Long, J. Guo and C. Wang, *Macromol. Biosci.*, 2019, **19**, 1800416.
76 L. Zhang, Z. Wang, R. Zhang, H. Yang, W. J. Wang, Y. Zhao, W. He, Z. Qiu, D. Wang, Y. Xiong, Z. Zhao and B. Z. Tang, *ACS Nano*, 2023, **17**, 25205–25221.
77 Y. Chen, P. A. Wilbon, J. Zhou, C. Wang, F. Chu and C. Tang, *Chem. Commun.*, 2012, **49**, 297–299.
78 Z. Li, W. Xu, Y. Wang, B. R. Shah, C. Zhang, Y. Chen, Y. Li and B. Li, *Carbohydr. Polym.*, 2015, **121**, 477–485.
79 W. B. Tan, S. Jiang and Y. Zhang, *Biomaterials*, 2007, **28**, 1565–1571.
80 A. M. Smith, H. Duan, A. M. Mohs and S. Nie, *Adv. Drug Delivery Rev.*, 2008, **60**, 1226–1240.
81 K. Pathakoti, H. M. Hwang, H. Xu, Z. P. Aguilar and A. Wang, *J. Environ. Sci.*, 2013, **25**, 163–171.
82 A. M. Derfus, W. C. W. Chan and S. N. Bhatia, *Nano Lett.*, 2004, **4**, 11–18.
83 J. Geys, A. Nemmar, E. Verbeken, E. Smolders, M. Ratoi, M. F. Hoylaerts, B. Nemery and P. H. M. Hoet, *Environ. Health Perspect.*, 2008, **116**, 1607–1613.
84 Y. Liu, N. Zhao and F.-J. Xu, *ACS Appl. Mater. Interfaces*, 2019, **11**, 34707–34716.
85 S. Rejinold N, K. P. Chennazhi, H. Tamura, S. V. Nair and J. Rangasamy, *ACS Appl. Mater. Interfaces*, 2011, **3**, 3654–3665.
86 J. M. Shen, L. Xu, Y. Lu, H. M. Cao, Z. G. Xu, T. Chen and H. X. Zhang, *Int. J. Pharm.*, 2012, **427**, 400–409.
87 J. S. Park, H. N. Yang, D. G. Woo, S. Y. Jeon and K. H. Park, *Biomaterials*, 2013, **34**, 8819–8834.
88 X. Q. Zhao, T. X. Wang, W. Liu, C. D. Wang, D. Wang, T. Shang, L. H. Shen and L. J. Ren, *J. Mater. Chem.*, 2011, **21**, 7240–7247.
89 S. Jiang, M. K. Gnanasammandhan and Y. Zhang, *J. R. Soc., Interface*, 2009, **1**, 3–18.
90 M. Gonçalves, D. Maciel, D. Capelo, S. Xiao, W. Sun, X. Shi, J. Rodrigues, H. Tomás and Y. Li, *Biomacromolecules*, 2014, **15**, 492–499.
91 L. Zha, B. Banik and F. Alexis, *Soft Matter*, 2011, **7**, 5908–5916.
92 Y. K. Shin, Y. R. Park, H. Lee, Y. Choi and J. B. Eom, *Pharmaceutics*, 2023, **15**, 930.

93 C. Ye, M. Cheng, L. Ma, T. Zhang, Z. Sun, C. Yu, J. Wang and Y. Dou, *ACS Appl. Mater. Interfaces*, 2022, **14**, 21822–21835.
94 R. Kawasaki, R. Ohdake, K. Yamana, T. Eto, K. Sugikawa and A. Ikeda, *J. Mater. Chem. B*, 2021, **9**, 6357–6363.
95 M. H. Cho, Y. Li, P. C. Lo, H. Lee and Y. Choi, *Nano-Micro Lett.*, 2020, **12**, 47.
96 K. Yang, L. Feng, X. Shi and Z. Liu, *Chem. Soc. Rev.*, 2012, **42**, 530–547.
97 Z. Khatun, M. Nurunnabi, M. Nafiujjaman, G. R. Reeck, H. A. Khan, K. J. Cho and Y. K. Lee, *Nanoscale*, 2015, **7**, 10680–10689.
98 H. Wang, J. Di, Y. Sun, J. Fu, Z. Wei, H. Matsui, A. Del, C. Alonso and S. Zhou, *Adv. Funct. Mater.*, 2015, **25**, 5537–5547.
99 H. Li, X. He, Y. Liu, H. Huang, S. Lian, S. T. Lee and Z. Kang, *Carbon*, 2011, **49**, 605–609.
100 C. Zhao, S. Sun, S. Li, A. Lv, Q. Chen, K. Jiang, Z. Jiang, Z. Li, A. Wu and H. Lin, *ACS Appl. Mater. Interfaces*, 2022, **14**, 10142–10153.
101 H. Wang, F. Ke, A. Mararenko, Z. Wei, P. Banerjee and S. Zhou, *Nanoscale*, 2014, **6**, 7443–7452.
102 D. Gyawali, J. P. Kim and J. Yang, *Bioact. Mater.*, 2018, **3**, 39–47.
103 S. Su, H. Wang, X. Liu, Y. Wu and G. Nie, *Biomaterials*, 2013, **34**, 3523–3533.
104 W. Wu, T. Zhou, A. Berliner, P. Banerjee and S. Zhou, *Chem. Mater.*, 2010, **22**, 1966–1976.
105 W. Wu, M. Aiello, T. Zhou, A. Berliner, P. Banerjee and S. Zhou, *Biomaterials*, 2010, **31**, 3023–3031.
106 L. Chambre, A. Degirmenci, R. Sanyal and A. Sanyal, *Bioconjugate Chem.*, 2018, **29**, 1885–1896.
107 M. Huo, J. Yuan, L. Tao and Y. Wei, *Polym. Chem.*, 2014, **5**, 1519–1528.
108 Y. Lin, C. Li, A. Liu, X. Zhen, J. Gao, W. Wu, W. Cai and X. Jiang, *Biomater. Sci.*, 2021, **9**, 1363–1373.
109 G. Zhang, M. Zhan, C. Zhang, Z. Wang, H. Sun, Y. Tao, Q. Shi, M. He, H. Wang, J. Rodrigues, M. Shen and X. Shi, *Adv. Sci.*, 2023, **10**, 2301759.
110 T. Xing, B. Lai and L. Yan, *Macromol. Chem. Phys.*, 2013, **214**, 578–588.
111 K. Bhattacharya, S. L. Banerjee, S. Das, S. Samanta, M. Mandal and N. K. Singha, *ACS Appl. Bio Mater.*, 2019, **2**, 2587–2599.
112 C. A. Choi, B. Ryplida, I. In and S. Y. Park, *Eur. J. Pharm. Sci.*, 2019, **134**, 256–265.
113 T. Shang, C. D. Wang, L. Ren, X. H. Tian, D. H. Li, X. B. Ke, M. Chen and A. Q. Yang, *Nanoscale Res. Lett.*, 2013, **8**, 1–8.
114 A. M. Lowman, T. D. Dziubla, P. Bures and N. A. Peppas, *Adv. Chem. Eng.*, 2004, **29**, 75–130.
115 Y. Qin, J. Chen, Y. Bi, X. Xu, H. Zhou, J. Gao, Y. Hu, Y. Zhao and Z. Chai, *Acta Biomater.*, 2015, **17**, 201–209.
116 R. B. Roemer, *Annu. Rev. Biomed. Eng.*, 1999, **1**, 347–376.
117 W. Wu, J. Shen, P. Banerjee and S. Zhou, *Biomaterials*, 2010, **31**, 8371–8381.
118 W. Wu, J. Shen, P. Banerjee and S. Zhou, *Adv. Funct. Mater.*, 2011, **21**, 2830–2839.
119 H. Zhu, Y. Li, R. Qiu, L. Shi, W. Wu and S. Zhou, *Biomaterials*, 2012, **33**, 3058–3069.
120 W. Wu, J. Shen, P. Banerjee and S. Zhou, *Biomaterials*, 2011, **32**, 598–609.
121 S. Quan, Y. Wang, A. Zhou, P. Kumar and R. Narain, *Biomacromolecules*, 2015, **16**, 1978–1986.
122 V. M. Vijayan, S. J. Shenoy, S. P. Victor and J. Muthu, *Colloids Surf., B*, 2016, **146**, 84–96.
123 V. M. Vijayan, S. J. Shenoy and J. Muthu, *Mater. Sci. Eng., C*, 2017, **76**, 490–500.
124 V. M. Vijayan, A. E. Beeran, S. J. Shenoy, J. Muthu and V. Thomas, *ACS Appl. Bio Mater.*, 2019, **2**, 757–768.
125 M. Pei, X. Jia, X. Zhao, J. Li and P. Liu, *Carbohydr. Polym.*, 2018, **183**, 131–139.
126 T. Jing, T. Li, Z. Ruan, Q. Cheng and L. Yan, *Macromol. Mater. Eng.*, 2018, **303**, 1800060.
127 J. Yang, M. H. Yao, L. Wen, J. T. Song, M. Z. Zhang, Y. D. Zhao and B. Liu, *Nanoscale*, 2014, **6**, 11282–11292.
128 S. Chen, Q. Bian, P. Wang, X. Zheng, L. Lv, Z. Dang and G. Wang, *Polym. Chem.*, 2017, **8**, 6150–6157.
129 H. Wang, J. Yi, S. Mukherjee, P. Banerjee and S. Zhou, *Nanoscale*, 2014, **6**, 13001–13011.
130 A. Jalalian, S. B. T. Mashohor, H. R. Mahmud, M. I. B. Saripan, A. R. B. Ramli and B. Karasfi, *Clin. Imaging*, 2013, **37**, 420–426.
131 M. Smeenge, M. Mischi, M. P. L. Pes, J. J. M. C. H. de la Rosette and H. Wijkstra, *World J. Urol.*, 2011, **29**, 581–587.
132 A. T. Ahuja, M. Ying, S. Y. Ho, G. Antonio, Y. P. Lee, A. D. King and K. T. Wong, *Cancer Imaging*, 2008, **8**, 48–56.
133 H. Yoon, K. A. Hallam, C. Yoon and S. Y. Emelianov, *IEEE Trans. Ultrason. Ferroelectr. Freq. Control*, 2018, **65**, 2277–2285.
134 Y. Zhai, W. Ran, J. Su, T. Lang, J. Meng, G. Wang, P. Zhang and Y. Li, *Adv. Mater.*, 2018, **30**, 1802378.
135 L. E. Theune, J. Buchmann, S. Wedepohl, M. Molina, J. Laufer and M. Calderón, *J. Controlled Release*, 2019, **311–312**, 147–161.
136 Y. Zhou, Y. Hu, W. Sun, B. Zhou, J. Zhu, C. Peng, M. Shen and X. Shi, *Nanoscale*, 2017, **9**, 12746–12754.
137 C. Zhang, W. Sun, Y. Wang, F. Xu, J. Qu, J. Xia, M. Shen and X. Shi, *ACS Appl. Mater. Interfaces*, 2020, **12**, 9107–9117.
138 D. H. Zhao, J. Yang, R. X. Xia, M. H. Yao, R. M. Jin, Y. D. Zhao and B. Liu, *Chem. Commun.*, 2018, **54**, 527–530.
139 R. Bar-Shalom, A. Y. Valdivia and M. D. Blaufox, *Semin. Nucl. Med.*, 2000, **30**, 150–185.
140 M. M. Khalil, J. L. Tremoleda, T. B. Bayomy and W. Gsell, *Int. J. Mol. Imaging*, 2011, **2011**, 1–15.
141 J. Lux, A. G. White, M. Chan, C. J. Anderson and A. Almutairi, *Theranostics*, 2015, **5**, 277–288.
142 S. Singh, B. Bingöl, A. Morgenroth, F. M. Mottaghy, M. Möller and J. Schmaljohann, *Macromol. Rapid Commun.*, 2013, **34**, 562–567.

143 S. Lee, S. W. Kang, J. H. Ryu, J. H. Na, D. E. Lee, S. J. Han, C. M. Kang, Y. S. Choe, K. C. Lee, J. F. Leary, K. Choi, K. H. Lee and K. Kim, *Bioconjugate Chem.*, 2014, **25**, 601–610.
144 N. Drude, S. Singh, O. H. Winz, M. Möller, F. M. Mottaghy and A. Morgenroth, *Biomacromolecules*, 2017, **18**, 2489–2498.
145 L. Kong, J. Zhu, H. Su, L. Zhao, Y. Lu, M. Zhu and W. Sun, *Front. Bioeng. Biotechnol.*, 2022, **10**, 973141.
146 S. Soni, A. K. Babbar, R. K. Sharma and A. Maitra, *J. Drug Targeting*, 2006, **14**, 87–95.
147 A. Gupta, S. Wang, A. Marko, P. Joshi, M. Ethirajan, Y. Chen, R. Yao, M. Sajjad, R. Kopelman and R. K. Pandey, *Theranostics*, 2014, **4**, 614–628.